Geochemistry Geophysics Geosystems G3
AN ELECTRONIC JOURNAL OF THE EARTH SCIENCES
Published by AGU and the Geochemical Society

Article
Volume 2
July 2, 2001
Paper number 2000GC000105
ISSN: 1525-2027

Across-arc geochemical trends in the Izu-Bonin arc: Contributions from the subducting slab

Alfred Hochstaedter, Jim Gill, Robert Peters, Phil Broughton, and Pete Holden
Earth Sciences Department, University of California, Santa Cruz, California 95064
(alfredh@marinetech.org; jgill@es.ucsc.edu)

Brian Taylor
School of Ocean and Earth Science and Technology, University of Hawaii, Honolulu, Hawaii 96822
(taylor@soest.hawaii.edu)

[1] **Abstract:** We propose that across-arc differences in the geochemistry of Izu-Bonin arc magmas are controlled by the addition of fertile-slab fluids to depleted mantle at the volcanic front, and residual-slab fluids to fertile mantle in the back arc without slab melting or contemporaneous back arc spreading. The arc consists of a volcanic front, an extensional zone, and seamount chains (the Western Seamounts) that trend into the Shikoku Basin. Each province produces a distinct suite of arc-like volcanic rocks that have relative Nb depletions and high ratios of fluid-mobile elements to high field strength elements. The volcanic front has the lowest concentrations of incompatible elements and the strongest relative enrichments of fluid-mobile elements (high U/Nb, Ba/Nb, Pb/Zr, Th/Nb, $^{206}Pb/^{204}Pb$, ε_{Nd}, and $^{87}Sr/^{86}Sr$). A fluid derived from both sediment and altered oceanic crust explains most of the slab-related characteristics of the volcanic front. The Western Seamounts and some of the extensional zone rocks have lower ε_{Nd}, $^{87}Sr/^{86}Sr$, $^{206}Pb/^{204}Pb$, Ba/Th, and U/Th; moderate Ba/Nb and U/Nb; and similar or higher Th/Nb and Th/Nd. Although the lower ε_{Nd} and higher Th/Nd tempt a sediment melt explanation, a lack of correlation between the strongest sediment proxies, such as ε_{Nd}, Th/Nb, and Ce/Ce*, precludes sediment melts. The subduction component for the Western Seamounts is probably a fluid dehydrated from a residual slab that was depleted in fluid-mobile elements beneath (as well as trenchward of) the volcanic front. This depleted fluid is added to elementally and isotopically more enriched mantle beneath the Western Seamounts.

Keywords: Trace element geochemistry; Izu-Bonin arc; Island arc; volcanic arc; isotope geochemistry.

Index terms: Minor and trace element composition; mineralogy and petrology; physics and chemistry of magma bodies.

Received August 31, 2000; **Revised** February 7, 2001; **Accepted** February 9, 2001; **Published** July 2, 2001.

Hochstaedter, A., J. Gill, R. Peters, P. Broughton, P. Holden, and B. Taylor, 2001. Across-arc geochemical trends in the Izu-Bonin arc: Contributions from the subducting slab, *Geochem. Geophys. Geosyst.*, vol. 2, Paper number 2000GC000105 [12,776 words, 15 figures, 3 tables]. Published July 2, 2001.

1. Introduction

[2] Convergent margin volcanism involves the transfer of chemical constituents from the subducting slab into the magma source region in the mantle wedge. One of the current debates centers on whether the transfer agent is a hydrous fluid, a silicate melt, or a combination

of both. Another is whether these melts or fluids derive from the altered oceanic crust, the overlying sedimentary cover, or both. Reasonable interpretations exist that support many of these options. For example, the occurrence of ^{10}Be in young arc volcanic rocks provides unambiguous evidence that a sedimentary component exists in many arc magmas [*Tera et al.*, 1986; *Morris and Tera*, 1989]. *Plank and Langmuir* [1993] showed that normalized concentration of certain elements in volcanic arc magmas correlate with the sediment-derived flux of these elements into the subduction zone, implying an important role for sediments in arc magma genesis.

[3] Other elemental systematics, such as B and ^{238}U excesses, show that slab-derived fluids are common transfer agents to the volcanic front [*Gill and Williams*, 1990; *Leeman et al.*, 1994; *Leeman*, 1996]. Detailed studies of individual arcs, such as the Marianas [*Elliott et al.*, 1997], Tonga [*Turner et al.*, 1997], and Aleutians ([*Class et al.*, 2000], have concluded that fluids from altered oceanic crust (AOC) and melts from subducted sediments provide the "slab components" in these arcs. These results have spurred experimental work into the question of fluid/solid and melt/solid partition coefficients under subduction zone conditions [*Brenan et al.*, 1994, 1995a, 1995b; *Ayers et al.*, 1997; *Stalder et al.*, 1998]. Often the strength of particular slab components in arc volcanic rocks correlates with distance to the trench or distance to the slab, as it does in the Kuriles [*Ryan et al.*, 1995] and New Britain [*Woodhead et al.*, 1998].

[4] The Izu-Bonin arc in the western Pacific offers an ideal place to investigate these issues for several reasons. Most importantly, the Izu-Bonin arc contains a wide zone of volcanism with both arc-like and back arc basin-like volcanism occurring behind the volcanic front, allowing us to investigate how the subduction component changes with depth to the slab as well as how the composition of magmas changes as extension begins. Furthermore, the Izu-Bonin arc is intraoceanic so that magma chamber level contamination by continental material is minimal.

[5] The Izu-Bonin arc is characterized by rapid subduction of old cold Pacific lithosphere beneath the relatively young warm Philippine Sea Plate in which back arc basins have formed as recently as 15 Ma. This combination minimizes the likelihood of melting of subducted components beneath the volcanic front (VF) and maximizes the likelihood of convection in the overlying mantle wedge [*Kincaid and Sacks*, 1997].

[6] The composition of the mantle wedge is at least as well known as for any other arc because oceanic basalts erupted onto the nearby Philippine Sea Plate have been well characterized both elementally and isotopically [*Hickey-Vargas*, 1991, 1998]. The wedge is "Indian" versus "Pacific" isotopically, increasing opportunity to distinguish the wedge from altered Pacific oceanic crust. Previous geochemical studies have shown that the Izu arc produces very depleted lavas, so that the effects of subduction component addition should be maximally identifiable. In an earlier paper, *Hochstaedter et al.* [2000] used major element and high field strength element (HFSE) concentrations to show that non-slab-related differences existed between volcanic front rocks and those erupted behind the volcanic front. Lavas erupted at the volcanic front had lower HFSE concentrations and different ratios than those from behind the volcanic front. Geochemical modeling indicated that these differences could be explained by magma generation and extraction behind the volcanic front despite the absence of contemporaneous back arc spreading. If the mantle wedge source regions were to then move toward the volcanic front due to

mantle wedge convection and then melt again, the resulting magmas would be depleted [*Hochstaedter et al.*, 2000].

[7] For the purposes of this paper, the words "enriched" and "depleted" will refer to variations in concentration of and ratios between the high field strength elements Ti, Zr, Hf, Nb, and Ta. Their concentrations and ratios in the Izu-Bonin arc range from more depleted than in normal mid-ocean ridge basalt (NMORB) to intermediate between enriched mid-ocean ridge basalt (EMORB) and oceanic island basalt (OIB). These differences are distinct from those variations related to the slab-derived component. Geochemical variations related to slab- or subduction-related processes will be referred to in terms of a strong or weak "slab signature" or "subduction signature" that can arise from any subducted material (e.g., various types of sediment and altered basalt) or agent of mass transfer into the overlying mantle (e.g., bulk addition, aqueous fluid, or silicate melt).

[8] The purpose of this paper is to use and extend the results of the previous study by documenting changes in the trace element and isotopic geochemistry of Izu-Bonin volcanic rocks with distance from the trench. In this paper we focus on those elements thought to be derived from the subducted slab. Our main conclusion is that geochemical variations require at least two different slab-derived components. Both of these components are probably fluids rather than melts, although their composition must change with depth of release from the slab.

2. Background

2.1. Tectonic and Geochemical Evolution

[9] In this section we describe the tectonic setting of the study area as well as the tectonic context of each of the rock types. The Izu-Bonin arc is formed by the subduction of the Pacific Plate beneath the Philippine Sea Plate. The subduction zone extends from the Izu Peninsula on the island of Honshu southward toward Iwo Jima where it meets the northern seamount province of the Mariana arc [*Yuasa and Nohara*, 1992]. Sediments on the downgoing Pacific Plate recently were collected at Ocean Drilling Program (ODP) Site 1149 [*Plank et al.*, 1999]. Detailed descriptions of the tectonic evolution of the Izu-Bonin arc are given by *Honza and Tamaki* [1985] on the basis of bathymetric and seismic profiles and by *Taylor* [1992] on the basis of additional seismic profiles, backscatter images, and ODP drilling. *Ishizuka et al.* [1998] measured K-Ar and Ar-Ar ages for a subset of the rocks for which elemental and isotopic data are reported here. *Hochstaedter et al.* [2000] summarized the tectonic and geochemical evolution of the Izu-Bonin arc. Interested readers are directed to these papers; only a brief synopsis is given here.

[10] Within the study area (Figure 1) the Izu-Bonin arc contains, from east to west, a volcanic front defined by several large but mostly submarine stratovolcanoes; an extensional zone defined by rift basins 10–60 km behind the volcanic front, fissure ridges, cinder cones aligned in a north-south manner, and north-south lineations on side-scan backscatter images; and four seamount chains that cross the arc in a northeast-southwest diagonal manner from within the extensional zone into the Shikoku Basin [*Morita*, 1994]. The rift basins contain Holocene lavas, but no back arc spreading has yet commenced.

[11] The VF of the Izu-Bonin arc (Figure 2) is one of the most depleted of all volcanic arcs. Concentrations in basalts (3–4 wt % MgO) are as low as 1.5 wt % Na_2O, 0.2–0.3 ppm Nb, 20–30 ppm Zr, 0.1 ppm Th, and ~8 times chondrite heavy rare earth elements

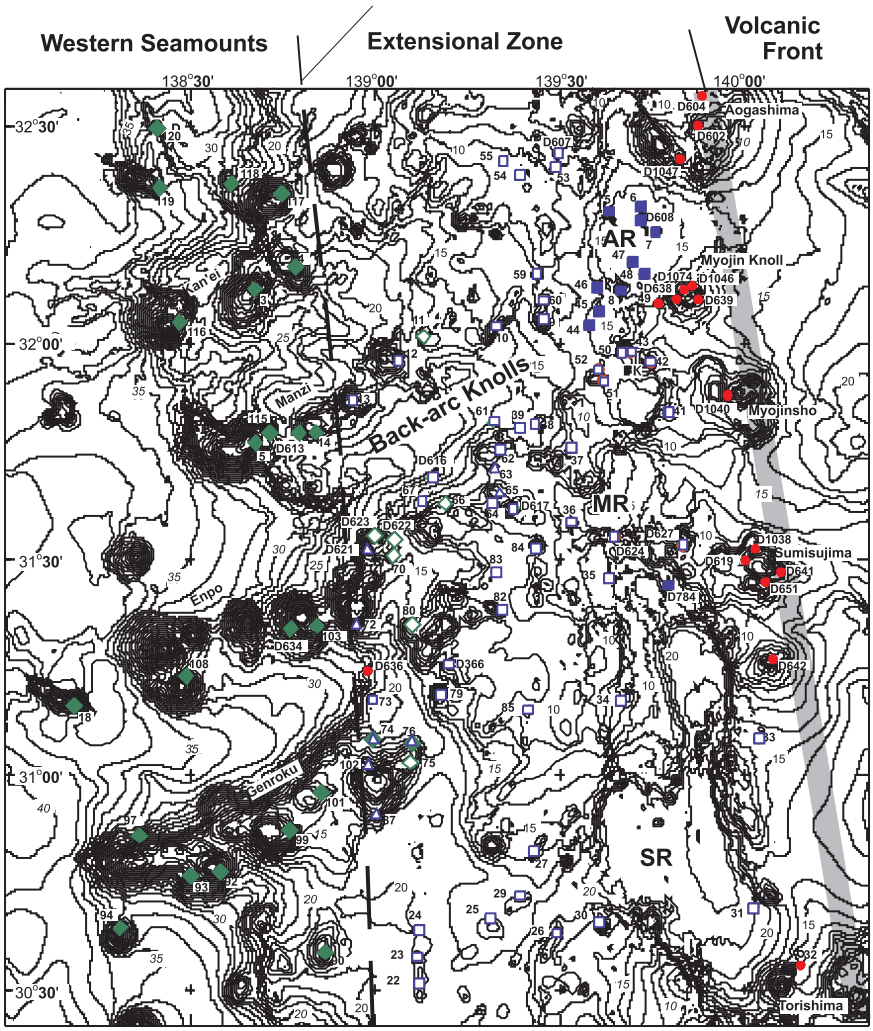

Figure 1. Map of the study area shows tectonic features, bathymetry, and sample locations. AR, MR, and SR represent the Aogashima, Miyojinsho, and Sumisu Rifts, respectively. Numbers D366 to D1074 refer to sites dredged by Geological Survey of Japan cruises. Sites designated by 3-120 were dredged by the R/V *Moana Wave*. The contour interval is 125 m, labeled in hundreds of meters. Circles, volcanic front; solid squares, active rift; open squares, back arc knolls; triangles, high K/Na knolls; open diamonds, Eastern Seamounts; solid diamonds, Western Seamounts. After *Hochstaedter et al.* [2000].

(REE). The lavas comprise a basalt through rhyolite suite that belongs to the low-K tholeiitic suite of *Gill* [1981] [*Fujimaki and Kurasawa*, 1980; *Ikeda and Yuasa*, 1989; *Yuasa and Nohara*, 1992; *Tatsumi et al.*, 1992; *Gill et al.*, 1992; *Takada et al.*, 1994; *Taylor and Nesbitt*, 1998]. These rocks also have low Nb/Zr (<0.025), and some have very low Nb/Ta (<13) values, indicating they were derived from sources more depleted than average NMORB (Figure 3) [*Hochstaedter et al.*, 2000]. The VF has been continuously active during the last 15 million years, as 0–15 Ma VF-derived turbidite and tephra layers occur in regional ODP sites *Gill et al.*, 1992, 1994; *Straub*, 1996].

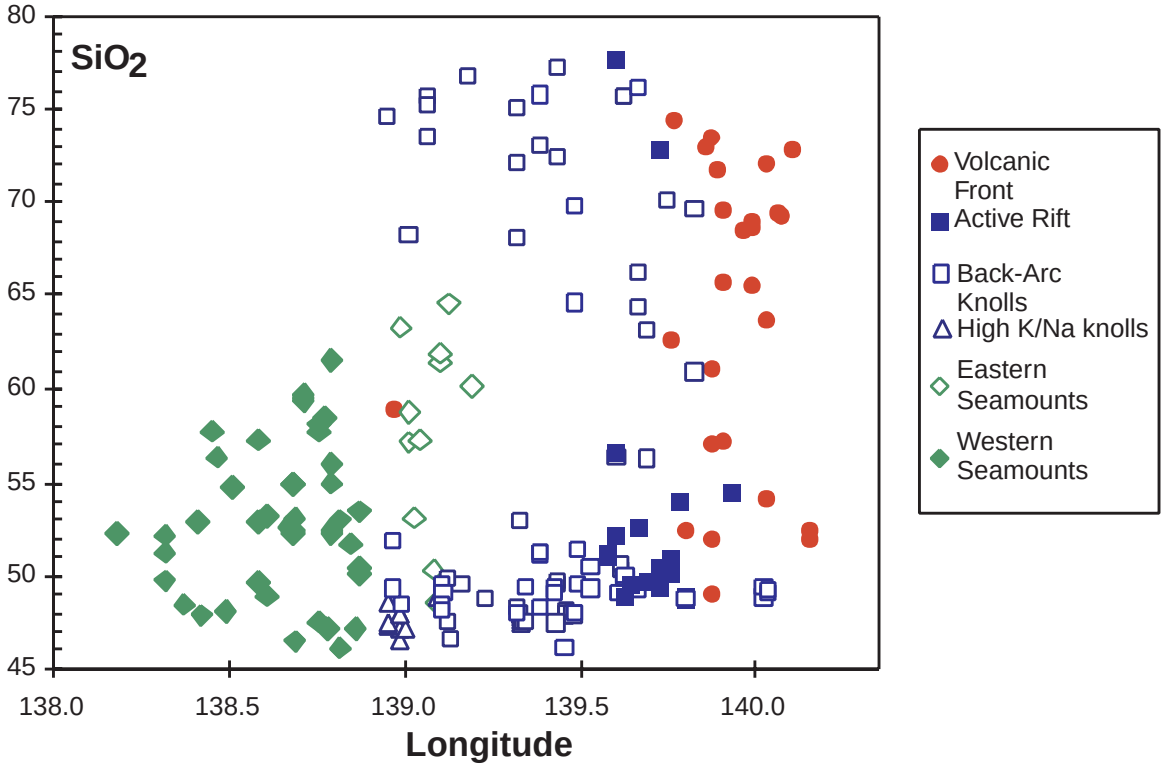

Figure 2. SiO_2 content of Izu-Bonin volcanic rocks versus longitude is proportional to distance from the trench or depth to the subducting slab. Symbols defined in the legend are used in Figures 3–15 and on Figure 1.

[12] The four across-arc seamount chains occur along southwesterly trends from just west of the VF to the Shikoku Basin. The portion of these chains that protrudes into the Shikoku Basin is referred to as the Western Seamounts (WS), whereas the portion that lies within the extensional zone is referred to as the Eastern Seamounts. K-Ar ages of seamount chain rocks range from 2.4 to 12.5 Ma, although ages >7 Myr are restricted to the WS [*Ishizuka et al.*, 1998]. The major element and HFSE chemistry of the western and eastern portions of the seamount chains are similar. They are arc-like in that andesite dominates the assemblage (Figure 2), they differentiate along a calc-alkaline trend, and they have high ratios of fluid-mobile elements relative to HFSE [*Hochstaedter et al.*, 2000]. They are also much more enriched than the VF, with HFSE concentrations and Nb/Ta and Nb/Zr ratios similar to EMORB (Nb/Ta > 13 and Nb/Zr > 0.025; see Figure 3). The principal geochemical difference between the Western and Eastern Seamounts is that Nd isotope ratios in the eastern ones are similar to those in the volcanic front, whereas they are lower in the Western Seamounts (Figures 3–5) [*Tatsumi et al.*, 1992].

[13] Extension of the Izu-Bonin arc began at ~2.8 Ma at this latitude [*Ishizuka et al.*, 1998]. Extension occurred over a wide area that is located mostly behind, but in places encompasses, the VF [*Taylor*, 1992; *Morita*, 1994]. Younger extensional features overprint the Eastern Seamounts in a region referred to as the back arc knolls zone [*Honza and Tamaki*, 1985; *Morita*, 1994; *Ishizuka et al.*, 1998]. The extensional zone also contains currently active

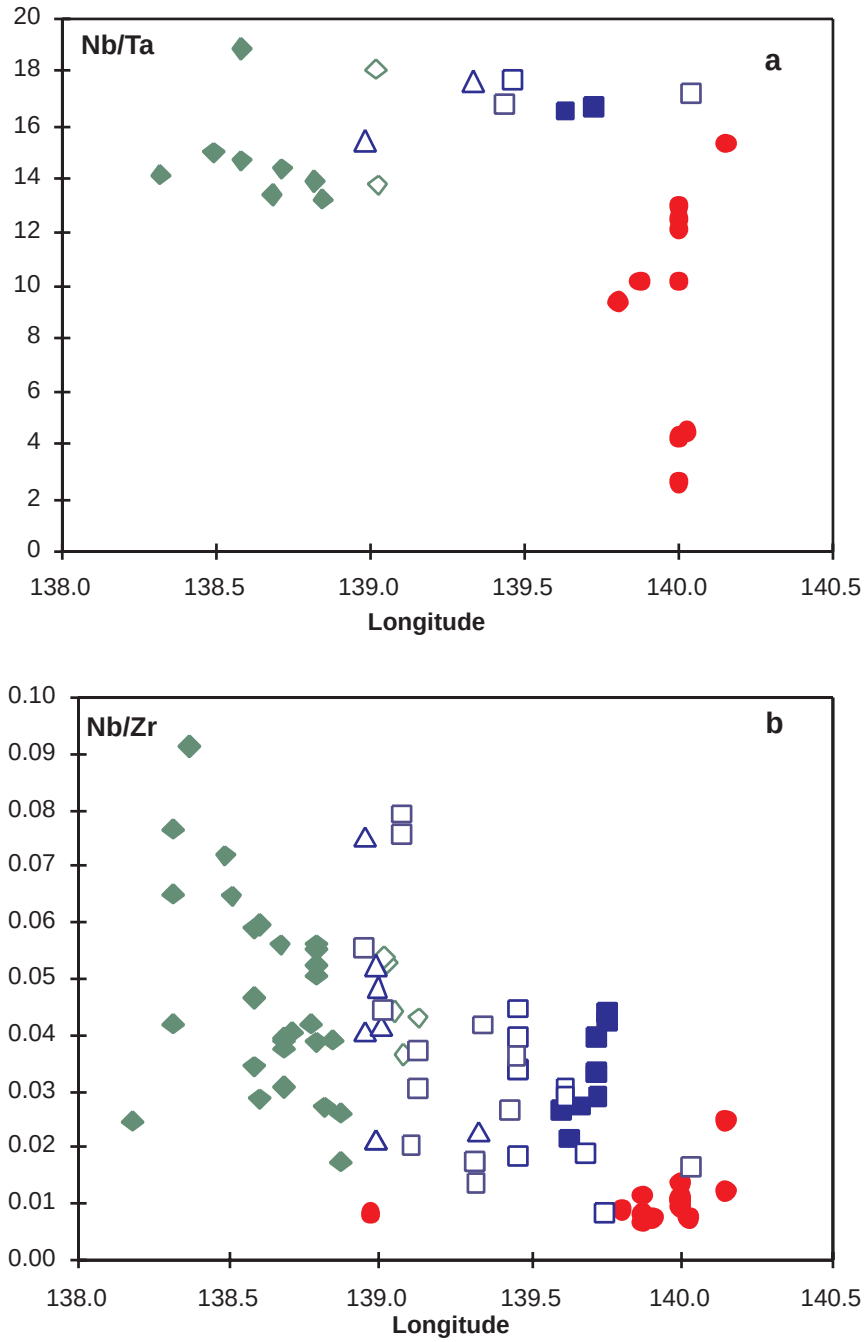

Figure 3. Increasing Nb/Ta and Nb/Zr across the arc from the VF to the WS suite indicates more enriched sources farther from the volcanic front. Low Nb/Ta in VF samples support the conclusions of *Hochstaedter et al.* [2000] that the most depleted lavas occur at the VF.

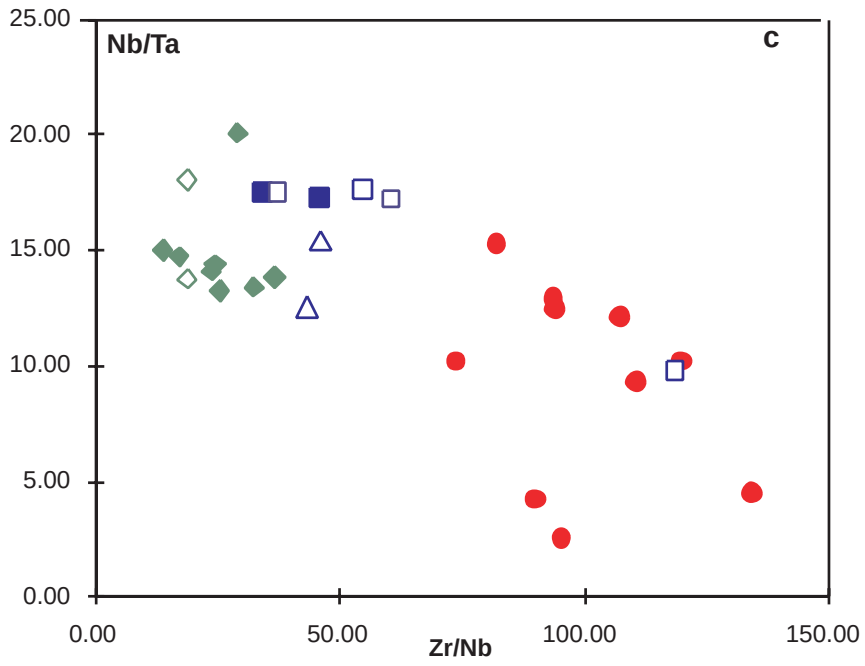

Figure 3. (continued)

rift basins, with rift axes 10–60 km behind the VF [*Taylor et al.*, 1990; *Klaus et al.*, 1992]. Three of these active rift basins are identified in Figure 1. The extension-related rocks are a bimodal basalt and rhyolite suite (Figure 2), have more subdued slab-related signatures than the VF rocks, and differentiate along more tholeiitic trends that are more similar to MORB than arcs [*Hochstaedter et al.*, 2000]. ALVIN collections from one of the rift basins, the Sumisu Rift (Figure 1), were studied in detail by *Fryer et al.* [1990] and *Hochstaedter et al.* [1990a, 1990b]. Three kinds of extension-related rocks are delineated on the diagrams in this paper: the active rifts, high K/Na basalts, and others (back arc knolls). Basalts in the active rifts in the east are <0.6 Ma and closest to EMORB in composition [*Hochstaedter et al.*, 1990a]. Our "back arc knolls" category includes most of the other volcanic rocks <2.8 Myr old from throughout the extensional zone, including ridges as well as seamounts. Our "high K/Na basalts" are a chemically distinct subset of back arc knolls basalts that have $Na_2O/K_2O < 3.4$ and $SiO_2 < 49$ wt % and were erupted mostly along the western margin of the extensional zone.

2.2. Element Affinities and Rationale for Data Presentation

[14] In order to distinguish between sources (sediments or altered oceanic crust) and transfer agents (sediment melt or hydrous fluids), specific elements, isotopes, or ratios need to be identified that represent each of these sources and transfer agents as well as processes occurring in the mantle wedge. On the basis of experimental work [*Brenan et al.*, 1994, 1995a, 1995b; *Ayers et al.*, 1997; *Stalder et al.*, 1998], studies of oceanic sediment [*Ben Othman et al.*, 1989; *Plank and Ludden*, 1992] and altered oceanic crust [*Staudigel et al.*, 1996], and results from studies of other subduction zones [*Stern et al.*, 1991; *Pearce and Parkinson*, 1993; *Davidson*, 1996; *Elliott et al.*,

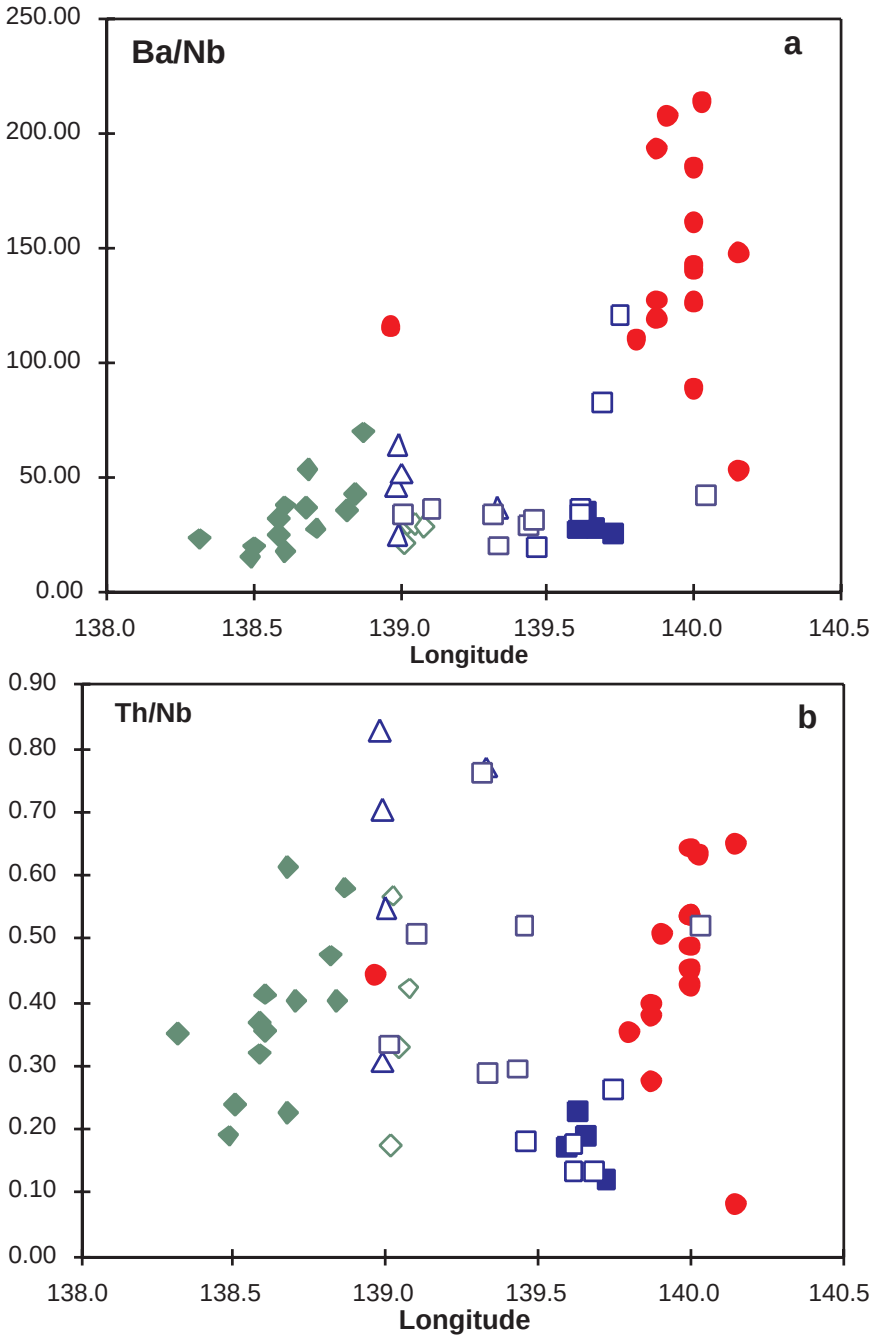

Figure 4. Fluid-mobile elements (such as Ba) are greatly enriched at the VF compared to the rest of the arc (Figure 4a), which has less variable enrichments of fluid-mobile elements. Elements enriched in sediments but not necessarily in fluids (such as Th and light rare earth elements (LREE)) are enriched at the VF, the inactive portion of the extensional zone, and the eastern portion of the Western Seamounts (WS). They are less enriched in the active rifts and in the far western portions of the WS (Figure 4b).

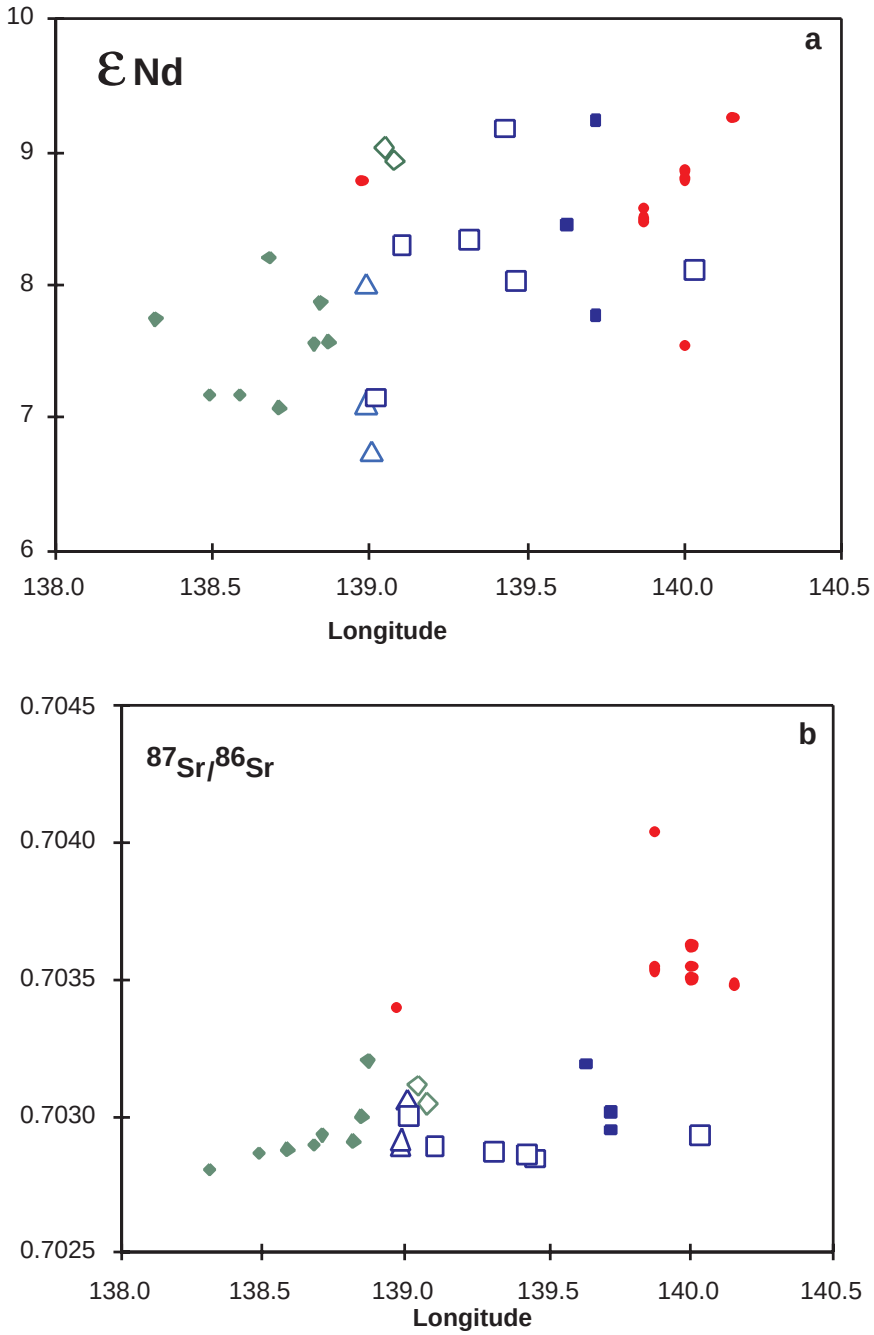

Figure 5. Isotopic values vary across the arc. Nd isotopes are relatively constant from the VF to the extensional zone but then decrease in the WS (Figure 7a). Sr (Figure 7b) and Pb (Figure 7c) isotopic ratios behave more like fluid-mobile elements with strong enrichments at the VF and relatively constant values across the rest of the arc.

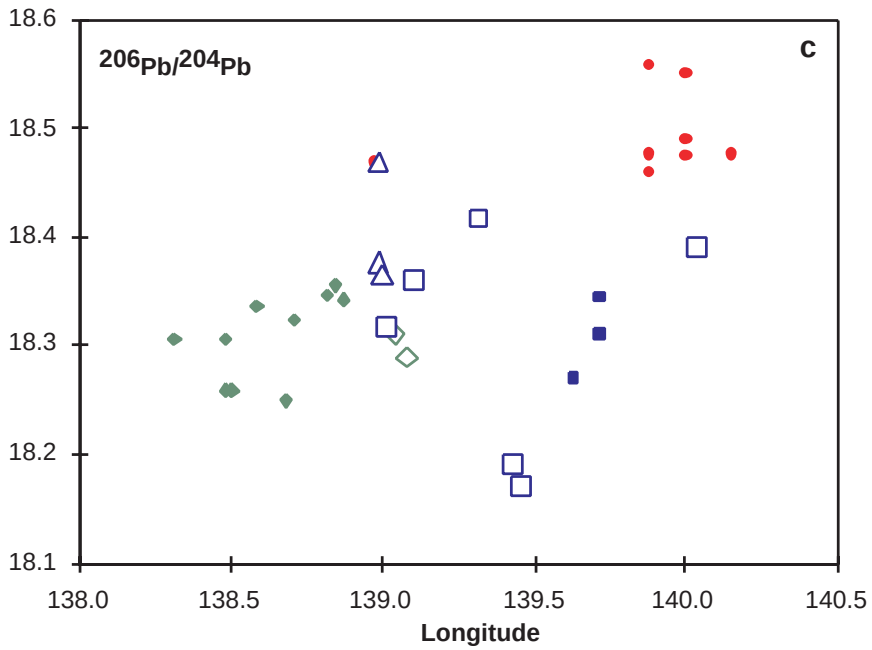

Figure 5. (continued)

1997; *Turner et al.*, 1997] a consensus has emerged among arc petrologists about which elements represent mantle processes and which can be used to investigate the roles of slab-derived components. The HFSE and heavy REE (Ta, Nb, Zr, Yb, and Y), for example, are not significantly mobile in fluids nor are they enriched in pelagic sediments and therefore may be used to study mantle processes [*Pearce and Parkinson*, 1993; *Davidson*, 1996], as has been done for this sample set by *Hochstaedter et al.* [2000]. Similarly, Th and the light REE (La-Nd) often are enriched in clastic sediments but are not highly mobile in fluids [*Brenan et al.*, 1994, 1995a, 1995b; *Ayers et al.*, 1997; *Elliott et al.*, 1997; *Stalder et al.*, 1998]. Thus they and Nd isotopes may be used to trace sediment addition without transfer by hydrous fluids. Elements such as Sr, Ba, Pb, U, and Cs are mobile in most fluids. Through comparison with Th and the LREE, these elements, including the isotopes of Sr and Pb, may be used to track the role of slab-derived hydrous fluids. We use Th/Nb as a proxy for sediments in this study. U/Nb and Ba/Nb have constant values in oceanic basalts and work well as fluid proxies.

3. Samples and Analytical Methods

[15] We conducted a thorough sampling program of the back arc region of the Izu-Bonin arc using the R/V *Moana Wave* in 1995 [*Hochstaedter et al.*, 2000]. One hundred twenty sites were dredged. Those sites from which rocks were recovered along with sites dredged by Geological Survey of Japan (GSJ) cruises using the R/V *Tansei-Maru* are shown in Figure 1. A representative suite from these two collections was analyzed for trace elements and isotopic ratios at University of California, Santa Cruz (UCSC) (Table 1). In addition, sediment samples (clay and chalk) from Deep Sea Drilling Project (DSDP) sites 195B and 198A were generously supplied by Bob Stern and included in our analytical program (Table 2). Nearly half of the samples that we analyzed from the volcanic front were dredged near Aogashima,

Table 1. Elemental and Isotopic Analyses for the Izu-Bonin Arc Region[a]

	Samples From Volcanic Front											
	32-1	32-3[b]	D636	D602a-1	D602a-2	D602-11	D604-4[b]	D638	D651-1	D9-21[b]	D7-153[b]	D9-26[b]
Latitude, °N	30.56	30.56	31.25	32.47	32.47	32.47	32.59	32.10	31.46	32.50	32.50	32.50
Longitude, °E	140.15	140.15	138.97	139.87	139.87	139.87	139.91	139.80	140.03	139.80	139.80	139.80
SiO_2	52.40	51.93	58.93	51.98	49.02	57.01	57.15	52.43	54.12	67.09	51.37	66.82
MgO	3.94	3.07	4.68	3.18	4.40	3.23	3.60	5.28	5.10	0.73	4.11	0.64
K_2O	0.27	0.17	0.38	0.11	0.29	0.28	0.42	0.17	0.31	0.42	0.29	0.53
K/Ar age			6.010									
Nb	0.321[c]	0.646	0.727[c]	0.220[c]	0.294[c]	0.591[c]	0.547[c]	0.415[c]	0.362[c]	0.92[c]	0.436[c]	0.97[c]
Ta	0.021				0.029			0.045	0.081	0.074	0.036	0.075
Zr	26.5	26.2	87.2	31.8	35.3	50.8	71.3	46.1	48.7	86.8	47.0	91.1
Hf	0.914	0.775	2.35	0.909	0.931	1.51	2.33	1.32	1.40	2.90	1.64	2.92
Rb	2.98	1.71	5.31	0.554	3.25	3.93	5.14	2.11	3.88	5.72	3.49	7.03
Sr	241	228	168	184	206	180	181	190	185	164	175	171
Cs	0.091	0.181	0.334	0.046	0.239	0.323	0.204	0.154	0.183			
Ba	47.3	33.7	83.4	42.5	34.9	75.0	113.4	45.6	77.2	131.0	80.5	136
La	2.13	0.924	3.06	0.826	1.34	2.25	2.72	1.76	2.05	4.55	2.27	4.69
Ce	5.70	3.25	10.25	3.00	4.26	6.70	8.31	5.65	5.98	13.0	6.93	13.3
Pr	1.02	0.654	1.55	0.631	0.795	1.22	1.59	1.02	1.10	2.22	1.27	2.26
Nd	5.31	3.68	7.93	3.54	4.38	6.54	8.79	5.42	5.81	12.6	7.68	12.5
Sm	1.71	1.39	2.54	1.36	1.58	2.28	3.19	1.90	2.02	3.77	2.53	4.09
Eu	0.644	0.623	0.892	0.582	0.683	0.870	1.15	0.784	0.736	1.14	0.882	1.29
Gd	2.28	2.04	3.43	2.04	2.25	3.23	4.60	2.64	2.86	5.57	3.79	5.50
Tb										0.973	0.670	0.958
Dy	2.52	2.58	4.09	2.56	2.79	3.92	5.62	3.16	3.47	5.87	4.07	6.91
Ho										1.504	1.03	1.50
Er	1.63	1.69	2.44	1.67	1.77	2.37	3.19	1.95	2.13	4.13	2.83	4.48
Tm										0.644	0.429	0.657
Yb	1.64	1.71	2.53	1.71	1.76	2.41	3.17	1.97	2.17	4.28	2.89	4.72
Lu										0.652	0.421	0.584
Pb	0.834	0.834	1.839	0.801	1.11	2.83	2.63	1.44	1.52	2.79	2.07	3.03
Th	0.208	0.052	0.321	0.060	0.117	0.222	0.277	0.146	0.229	0.547	0.235	0.549
U	0.189	0.039	0.150	0.073	0.128	0.116	0.359	0.0696	0.196	0.214	0.136	0.226
$^{143}Nd/^{144}Nd$		0.513113	0.513088	0.513074	0.513072	0.513078						
ε_{Nd}		9.3	8.8	8.5	8.5	8.6						
$^{87}Sr/^{86}Sr$		0.703480	0.703397	0.704036	0.703532	0.703548						
$^{206}Pb/^{204}Pb$		18.48	18.47	18.56	18.48	18.46						
$^{207}Pb/^{204}Pb$		15.57	15.56	15.58	15.54	15.53						
$^{208}Pb/^{204}Pb$		38.39	38.45	38.51	38.39	38.36						

Table 1. (continued)

	Samples From Volcanic Front			Samples From Active Rift				Samples From Low Na/K Knolls				
	D8-1[b]	D7-201[b]	D7-002[b]	5-3	8-3	45-3	48-2	102-3	74-3	D621-6	87-3	63-8
Latitude,°N	32.50	32.50	32.50	32.30	32.12	32.07	32.16	31.03	31.08	31.53	30.91	31.72
Longitude, °E	139.80	139.80	139.80	139.63	139.66	139.60	139.73	138.98	138.99	138.99	139.00	139.33
SiO_2	55.50	48.00	49.08	48.99	52.60	56.57	49.82	47.17	47.84	46.65	47.16	47.73
MgO	2.21	4.90	3.85	8.06	3.69	3.18	7.49	8.70	6.19	8.34	5.57	6.68
K_2O	0.29	0.03	0.14	0.23	0.40	0.43	0.20	0.81	0.65	0.58	0.93	0.55
K/Ar age								1.53	2.05	0.99	1.78	
Nb	0.590[c]	0.242[c]	0.375[c]	0.940[c]	2.13	2.51	1.30[c]	0.847[c]	2.84	0.813[c]	1.96	1.06[c]
Ta	0.231	0.057	0.037	0.057			0.078	0.055				0.060
Zr	56.3	21.8	27.8	45.3	78.1	93.8	47.2	39.1	58.4	37.4	47.1	43.2
Hf	1.85	0.731	0.930	1.27	2.19	2.41	1.33	1.17	1.72	1.18	1.70	1.25
Rb	4.25	3.26	2.96	2.97	5.26	5.80	2.12	18.3	11.0	10.5	21.7	14.9
Sr	182	174	189	218	271	266	214	485	464	436	531	339
Cs				0.117	0.193	0.214	0.081	0.332	0.301	0.108	0.670	0.447
Ba	94.9	21.3	47.2	34.4	58.6	67.5	33.8	39.1	71.0	51.9	101	36.3
La	2.81	1.15	1.75	2.49	4.66	5.12	2.93	7.52	8.99	6.90	11.56	5.21
Ce	8.31	3.36	4.90	7.39	13.4	14.8	8.54	18.4	19.5	16.7	24.0	12.9
Pr	1.48	0.594	0.829	1.28	2.27	2.53	1.48	3.01	3.04	2.69	4.26	2.11
Nd	8.83	3.46	4.62	6.58	11.6	13.0	7.52	14.6	14.2	12.6	20.4	10.1
Sm	2.78	1.08	1.46	2.10	3.58	3.93	2.30	3.73	3.46	3.12	5.00	2.76
Eu	0.944	0.420	0.545	0.815	1.34	1.52	0.877	1.18	1.19	1.01	1.54	0.940
Gd	4.02	1.67	2.14	2.77	4.60	5.03	3.00	3.95	3.89	3.44	5.18	3.23
Tb	0.712	0.303	0.375									
Dy	4.38	1.81	2.29	3.08	4.95	5.34	3.22	3.17	3.53	3.15	4.32	3.19
Ho	1.11	0.472	0.587									
Er	3.06	1.27	1.60	1.86	2.74	2.94	1.91	1.73	1.99	1.77	2.26	1.86
Tm	0.476	0.200	0.251									
Yb	3.20	1.32	1.63	1.82	2.68	2.88	1.86	1.58	1.92	1.67	2.11	1.79
Lu	0.473	0.198	0.242									
Pb	2.21	0.483	1.21	1.61	1.44	1.44	0.659	0.535	1.186	0.739	1.56	1.17
Th	0.294	0.119	0.279	0.222	0.400	0.429	0.164	0.703	0.867	0.571	1.072	0.772
U	0.128	0.054	0.090	0.103	0.230	0.184	0.078	0.251	0.278	0.267	0.344	0.233
$^{143}Nd/^{144}Nd$	0.513089	0.513092	0.513024	0.513071				0.513002		0.513048	0.512984	
ε_{Nd}	8.8	8.9	7.5	8.4				7.1		8.0	6.7	
$^{87}Sr/^{86}Sr$	0.703548	0.703506	0.703622	0.703189				0.702895		0.702917	0.703062	
$^{206}Pb/^{204}Pb$	18.47	18.49	18.55	18.27				18.38		18.47	18.36	
$^{207}Pb/^{204}Pb$	15.55	15.55	15.57	15.50				15.56		15.56	15.51	
$^{208}Pb/^{204}Pb$	38.42	38.44	38.49	38.12				38.22		38.23	38.13	

Table 1. (continued)

	Samples From Back-Arc Knolls											
	38-1[b]	62-3[b]	D623-1	9-6[b]	60-1[b]	24-1[b]	25-8[b]	33-1[b]	41-1	43-8[b]	51-6	52-3
Latitude, °N	31.82	31.76	31.57	32.06	32.10	30.65	30.66	31.09	31.84	31.98	31.92	31.94
Longitude, °E	139.44	139.34	139.01	139.46	139.46	139.11	139.32	140.04	139.79	139.69	139.62	139.60
SiO_2	49.57	47.59	68.23	48.03	46.18	48.48	48.03	49.02	48.75	56.28	50.59	56.32
MgO	7.66	5.22	1.13	7.41	6.89	7.84	6.68	10.29	6.35	2.86	6.29	4.98
K_2O	0.38	0.61	2.25	0.17	0.23	0.37	0.49	0.23	0.17	0.24	0.19	0.38
K/Ar age		0.54	2.49			2.62				0.643		
Nb	1.45[c]	2.58	6.83[c]	0.694[c]	1.43	0.802	0.639	0.487[c]	0.292[c]	0.849	1.03	1.80
Ta	0.087			0.039				0.028	0.030			
Zr	56.5	62.1	155	38.1	39.5	39.4	36.3	29.6	34.7	44.8	33.8	61.7
Hf	1.53	1.80	3.53	1.01	1.21	1.15	1.11	0.84	1.016	1.49	1.06	1.71
Rb	6.69	15.2	37.5	1.64	7.07	7.09	12.3	4.32	2.23	2.81	2.37	6.38
Sr	308	362	324	359	358	410	440	282	209	173	205	186
Cs	0.206	0.416	0.904	0.045	0.569	0.160	0.710	0.098	0.130	0.288	0.140	0.255
Ba	43.2	50.3	223	12.7	44.5	28.3	21.4	20.4	35.0	69.6	36.4	60.8
La	4.55	6.87	15.4	2.24	6.76	5.08	5.57	3.55	1.22	1.79	1.75	2.92
Ce	11.8	17.1	32.9	7.15	12.3	11.8	14.3	8.84	4.12	5.84	5.50	8.23
Pr	1.93	2.88	4.41	1.31	2.07	2.03	2.23	1.44	0.82	1.16	1.00	1.38
Nd	9.32	14.2	18.1	6.99	10.2	10.2	10.6	6.74	4.49	6.67	5.42	6.72
Sm	2.60	3.99	3.83	2.17	2.88	2.72	2.63	1.79	1.62	2.56	1.88	2.06
Eu	0.947	1.37	1.17	0.851	1.04	0.931	0.920	0.644	0.674	1.00	0.782	0.740
Gd	3.19	4.78	3.97	2.71	3.77	3.09	2.95	2.21	2.34	3.84	2.66	2.74
Tb												
Dy	3.18	4.63	3.70	2.95	3.93	3.04	2.83	2.41	2.75	4.78	3.10	3.15
Ho												
Er	1.86	2.48	2.28	1.77	2.27	1.81	1.70	1.55	1.72	2.81	1.91	1.97
Tm												
Yb	1.80	2.34	2.56	1.68	2.12	1.76	1.62	1.52	1.69	2.88	1.87	2.06
Lu												
Pb	1.04	0.994	3.151	0.132	8.15	0.609	0.526	0.348	0.597	2.807	0.935	1.204
Th	0.443	0.745	2.276	0.125	0.744	0.406	0.486	0.253	0.076	0.112	0.138	0.314
U	0.137	0.286	0.725	0.054	1.32	0.121	0.162	0.104	0.054	0.558	0.066	0.127
$^{143}Nd/^{144}Nd$			0.513005	0.513049		0.513063	0.513065	0.513053	0.513080			
ε_{Nd}			7.2	8.0		8.3	8.3	8.1	8.6			
$^{87}Sr/^{86}Sr$			0.703000	0.702836		0.702886	0.702865	0.702921	0.703282			
$^{206}Pb/^{204}Pb$			18.32	18.17		18.36	18.42	18.39	18.46			
$^{207}Pb/^{204}Pb$			15.54	15.48		15.52	15.55	15.55	15.53			
$^{208}Pb/^{204}Pb$			38.19	37.93		38.13	38.23	38.21	38.34			

Table 1. (continued)

	Samples From Western Seamounts, Genroku Chain					Samples From Western Seamounts, Enpo Chain		Samples From Western Seamounts, Manzi Chain		
	90-1	92-2	92-7	93-3	94-1	103-3	108-6	15-2	14-1	115-2
Latitude,°N	30.59	30.78	30.78	30.77	30.65	31.35	31.24	31.77	31.81	31.80
Longitude, °E	138.87	138.58	138.58	138.50	138.31	138.84	138.49	138.68	138.82	138.71
SiO_2	53.47	57.24	49.69	54.69	49.75	51.77	48.14	54.87	53.05	59.38
MgO	4.02	3.52	5.82	4.46	6.15	3.86	12.25	1.65	4.47	2.46
K_2O	0.75	1.52	0.87	0.94	0.62	0.92	0.47	2.70	0.92	1.88
K/Ar age	12.50	6.04		6.75	4.82	4.54	3.65			8.89
Nb	1.14	7.06[c]	2.05[c]	5.84	2.87[c]	2.94[c]	3.94[c]	4.57[c]	2.56[c]	5.55[c]
Ta		0.480	0.109		0.203	0.222	0.263	0.341	0.184	0.385
Zr	64.2	120	63.3	90.3	68.0	74.6	54.7	147	93.9	136.4
Hf	1.87	2.95	1.87	2.36	1.92	2.11	1.57	3.26	2.44	3.44
Rb	12.5	37.6	9.68	21.9	11.6	18.3	6.97	30.2	17.9	35.0
Sr	249	425	591	423	422	422	270	402	326	380
Cs	0.380	1.21	0.038	0.679	0.377	0.532	0.226	0.057	0.585	1.201
Ba	79.1	176	70.9	116	67.3	125	58.9	245	90.7	152
La	4.35	13.1	8.66	9.89	9.54	8.05	5.48	14.1	7.35	13.8
Ce	11.6	26.6	21.5	21.7	18.4	19.6	12.5	30.9	18.4	31.2
Pr	1.78	3.60	3.45	3.06	2.91	2.78	1.92	3.86	2.63	4.50
Nd	8.95	15.2	16.6	13.6	13.5	13.4	8.97	16.2	12.3	20.3
Sm	2.72	3.50	4.26	3.41	3.51	3.68	2.53	3.62	3.34	5.12
Eu	0.902	1.15	1.38	1.13	1.19	1.22	0.855	1.22	1.08	1.61
Gd	3.47	3.93	4.63	3.95	4.26	4.36	3.03	4.02	3.95	5.79
Tb										
Dy	3.92	3.66	4.13	3.80	4.13	4.46	3.22	3.73	4.06	5.64
Ho										
Er	2.35	2.17	2.24	2.18	2.36	2.51	1.92	2.18	2.34	3.08
Tm										
Yb	2.36	2.25	2.15	2.16	2.27	2.46	1.92	2.22	2.36	3.07
Lu										
Pb	1.59	3.16	0.861	1.99	1.23	1.84	1.14	3.82	2.27	3.61
Th	0.660	2.25	0.801	1.40	1.01	1.18	0.746	2.80	1.21	2.23
U		0.69	0.280	0.404	0.250	0.359	0.196	0.842	0.345	0.634
$^{143}Nd/^{144}Nd$	0.513026	0.513006			0.513035	0.513041	0.513006		0.513025	0.513001
ε_{Nd}	7.6	7.2			7.8	7.9	7.2		7.6	7.1
$^{87}Sr/^{86}Sr$	0.703204	0.702880			0.702800	0.702997	0.702860		0.702910	0.702930
$^{206}Pb/^{204}Pb$	18.34	18.34		18.26	18.31	18.35	18.31		18.35	18.32
$^{207}Pb/^{204}Pb$	15.52	15.54		15.49	15.51	15.52	15.54		15.56	15.56
$^{208}Pb/^{204}Pb$	38.19	38.25		38.08	38.17	38.25	38.23		38.29	38.26

Table 1. (continued)

	Samples From Western Seamounts, Kenei Chain				Samples From Eastern Seamounts				Standard Data		
	3-1[b]	3-2	118-2	118-9	D622-3	D623-10	70-2	75-1	BIR	JB-2	Coefficient of Variation
Latitude, °N	32.13	32.13	32.37	32.37	31.53	31.57	31.52	31.05			
Longitude, °E	138.68	138.68	138.60	138.60	139.02	139.01	139.04	139.08			
SiO_2	54.97	52.35	48.89	53.25	53.13	57.17	57.29	50.36			
MgO	5.40	4.16	10.08	3.50	2.29	4.21	3.70	4.97			
K_2O	1.16	1.94	0.35	2.50	1.93	0.86	1.59	0.61			
K/Ar age						2.39	3.64	5.11			
Nb	3.33	4.58	1.39	7.93	5.64[c]	4.84[c]	5.26	2.52	0.494	0.459	1.3
Ta					0.409	0.267			0.048	0.041	1.4
Zr	83.1	121.6	47.8	132.9	106.5	89.6	118.7	68.6	15.1	47.9	1.0
Hf		1.46	1.40	3.14	2.25	2.69	2.18	2.03	0.649	1.55	0.6
Rb		33.9	6.10	38.1	25.5	10.4	19.7	12.1	0.505	6.62	1.2
Sr		431	233	405	471	493	296	334	110	180	1.1
Cs		0.423	0.182	0.271	0.241	0.268	0.594	0.419			
Ba		167	24.3	297	164	105	154	71.2	6.54	218	1.2
La		12.0	3.92	14.7	13.4	11.1	9.59	6.17	0.626	2.28	0.7
Ce		25.6	10.0	28.2	33.2	29.4	21.4	15.1	1.89	6.48	0.9
Pr		3.71	1.59	3.88	3.83	4.47	3.08	2.26	0.365	1.13	0.4
Nd		16.5	7.81	16.3	16.6	21.5	13.7	10.6	2.4	6.34	0.3
Sm		4.10	2.35	3.83	3.85	5.56	3.32	2.96	1.09	2.20	0.6
Eu		1.30	0.829	1.21	1.37	1.82	0.992	0.956	0.486	0.772	1.1
Gd		4.57	2.96	4.27	4.16	6.14	3.80	3.47	1.84	3.17	1.1
Tb									0.347	0.552	1.1
Dy		4.29	3.22	4.05	3.77	5.93	3.77	3.62	2.66	4.06	0.9
Ho									0.57	0.870	0.8
Er		2.32	1.91	2.31	2.12	3.15	2.19	2.11	1.72	2.59	0.6
Tm									0.24	0.370	0.6
Yb		2.23	1.89	2.35	2.07	3.07	2.23	2.10	1.77	2.67	0.5
Lu									0.22	0.331	0.5
Pb		2.77	0.844	3.358	6.46	2.18	2.209	1.587	3.09	5.27	0.3
Th		1.03	0.572	2.805	3.20	0.849	1.727	1.063	0.043	0.291	0.4
U		0.243	0.158	0.780	0.424	0.300	0.493	0.288	0.01	0.168	0.4
$^{143}Nd/^{144}Nd$	0.513059						0.513101	0.513096			
ε_{Nd}	8.2						9.0	8.9			
$^{87}Sr/^{86}Sr$	0.702896						0.703109	0.703043			
$^{206}Pb/^{204}Pb$	18.25						18.31	18.29			
$^{207}Pb/^{204}Pb$	15.48						15.48	15.49			
$^{208}Pb/^{204}Pb$	38.04						38.13	38.15			

the VF island most like the WS in some geochemical ratios (lowest Ba/Zr, Pb/Nb, and ε_{Nd} ratios) yet in which HFSE concentrations are together with the island of Torishima the lowest in the arc and Pb is most like sediment isotopically [*Taylor and Nesbitt*, 1998]. All sample names beginning with "D" are from the GSJ and were crushed in agate. The others were dredged by us and crushed in tungsten carbide (WC); for some a separate aliquot was crushed in alumina.

[16] All elemental analyses reported here were analyzed using a Finnigan Element inductively coupled plasma-mass spectrometer (ICP-MS) at UCSC. Most analyses were made at the same time, by the same methods, and with the same precision and accuracy as those reported by *Hochstaedter et al.* [2000], using samples that were crushed in WC. All samples were run in at least duplicate calibrations and average replications differed by <1% for Nb and Yb. Information about precision and accuracy is given in Table 1.

[17] Samples for which Ta and additional heavy REE concentrations are reported in Table 1 were analyzed somewhat differently. They were recrushed in alumina, dissolved in a HF-HNO_3-$HClO_4$ mixture, spiked with internal standards, diluted by a factor of 1000, and calibrated to synthetic rather than rock standards. Most of them were analyzed solely for Nb and Ta to avoid effects of contamination during crushing; some also were analyzed for all elements reported in Table 1. Precision and accuracy information in Table 1 for Nb, Ta, Tb, Ho, Tm, and Lu refer to this analytical procedure. Our results for JB2 (which is from the Izu volcanic front) and BIR using both procedures generally agree with those of *Taylor and Nesbitt* [1998] and *Elliott et al.* [1997] to within 10%, although they differ from results for HFSE in JB2 on the home page of the Geological Survey of Japan.

[18] Table 1 contains additional trace element and Sr-Nd-Pb isotope analyses of the same samples reported by *Hochstaedter et al.* [2000] and the same kind of information for 17 additional samples. The new Nb concentrations are ~500 ppb lower than those of *Hochstaedter et al.* [2000], mostly reflecting the effect of grinding in WC versus alumina at UCSC. The difference is well within the concentration range of the samples considered by *Hochstaedter et al.* [2000] and does not alter their conclusions based on HFSE systematics.

[19] For isotopic analysis, chemical separation of REE, Sr, and Pb from whole-rock samples followed standard anion and cation resin ion exchange procedures. Nd was separated from the REE using LnSpec (Eichrom Industries). Blanks were <100 ng in all cases. Isotope ratios were measured on a Micromass Sector 54 equipped with nine third-generation Faraday collectors. Measured $^{143}Nd/^{144}Nd$ for La Jolla and $^{87}Sr/^{86}Sr$ for SRM 987 were 0.511858 ± 10 (n = 8) and 0.710254 ± 12 (n = 10), respectively. Common Pb isotope ratios were corrected for mass fractionation by 1.4‰ per amu

Notes to Table 1:

[a]All elemental concentrations (ppm) were analyzed by inductively coupled plasma-mass spectrometry (ICP-MS) by Hochstaedter from WC crushed powders except the following: All Japanese dredge samples (designated by a "D" before the sample name) were crushed by agate and then analyzed by A. Hochstaedter, except if Ta (but not Tb, Ho, Tm, or Lu) analyses are shown, the sample was recrushed in Al (*Moana Wave* samples only), after which, Nb and Ta but no other elements were reanalyzed by P. Holden. If Ta, Tb, Ho, Tm, and Lu analyses are shown, all of the elements, except Zr, were measured by ICP-Ms by Holden. The element Zr was analyzed by X-ray fluorescence (XRF) [*Hochstaedter et al.*, 2000].

[b]These samples were not previously reported by *Hochstaedter et al.* [2000].

[c]Values designate non-WC crushing for these particular samples; all Ta analyses represent non-WC crushing.

with respect to SRM 981 [*Todt et al.*, 1984]. All isotope ratios were measured in static mode.

4. Results

[20] The main purpose of this paper is to investigate the variation in strength and type of subduction signature across the arc. Selected attributes are plotted against longitude (which is proportional to distance from the trench) in Figures 3–5. In general, unequivocal slab signatures are strongest at the volcanic front and weaker behind the volcanic front. In terms of fluid-mobile elements (e.g., U, Pb, and Ba) the volcanic front has significantly higher fluid-mobile element/Nb ratios than anything behind the volcanic front, with few exceptions (Figure 4a). The region just behind the VF, within the active rifts, and the far western seamounts have the weakest fluid signatures, though still higher than in either MORB or OIB. The signature gets stronger at the western edge of the extensional zone, where the high K/Na basalts erupted, and then weakens again along the chains with distance from the VF. Some exceptions to this rule include a few samples from small stratovolcanoes located just behind the volcanic front but between the active rift basins (e.g., sample 41-1). The genesis of these rocks may have more in common with the VF than with the extensional zone.

[21] Some sediment-related element ratios, such as Th/Nb, are similar across the arc apart from the lowest values occurring in the active rifts. Others ratios, such as Th/Nd, suggest more sediment in the WS. This variation differs somewhat from the fluid-mobile elements shown in Figure 4. All of the ratios are higher than in MORB or OIB, even though they are not expected to be fractionated during mantle melting. A peak in Th/Nb is reached at the western half of the extensional zone. The values then gradually decrease with distance away from the trench along the across-arc seamount chains (Figure 4). The gradual decrease along the WS segment of the across-arc seamount chains may be due to increasing Nb concentrations along these chains.

[22] Our radiogenic isotope ratios are similar to those of *Taylor and Nesbitt* [1998] but extend to more extreme end-members. Pb in our VF samples from near Aogashima is slightly more radiogenic, whereas Sr in our WS samples is substantially less radiogenic than in similar samples measured by *Taylor and Nesbitt* [1998]. The radiogenic isotopes show patterns somewhat similar to those of the trace-element tracers. For Sr and Pb the volcanic front has higher isotopic ratios than anything behind it, isotopic ratios are broadly similar in both the extensional zone and WS, and they gradually decline away from the trench within the WS (Figure 5). Pb is even more similar to the fluid-mobile trace elements than Sr because a $^{206}Pb/^{204}Pb$ maximum occurs in the high K/Na basalts erupted at the beginning of rifting, whereas this maximum does not occur for $^{87}Sr/^{86}Sr$. In contrast, ε_{Nd} values in extensional zone rocks other than the high K/Na basalts are similar to those of volcanic front rocks, whereas values in the WS decline with distance from the volcanic front. Thus mantle sources within the extensional zone and volcanic front must be similar isotopically but different from those of the WS. As a result, for the Izu arc, there is a positive correlation between $^{87}Sr/^{86}Sr$ and $^{143}Nd/^{144}Nd$ (Figure 6a) and between $^{206}Pb/^{204}Pb$ and $^{143}Nd/^{144}Nd$ ratios. Sr-Nd-Pb isotope ratios for some samples from the extensional zone overlap with those of Philippine Sea Plate basalts [*Hickey-Vargas*, 1998], but most of the VF lavas are displaced to higher $^{87}Sr/^{86}Sr$, whereas most of the WS and high K/Na basalts are displaced to lower ε_{Nd} (Figure 6a). All of the Pb isotopic values plot above the Northern Hemisphere regression line (NHRL) in $^{208}Pb/^{206}Pb$ [*Hart*, 1984] (Figure 6b). Most

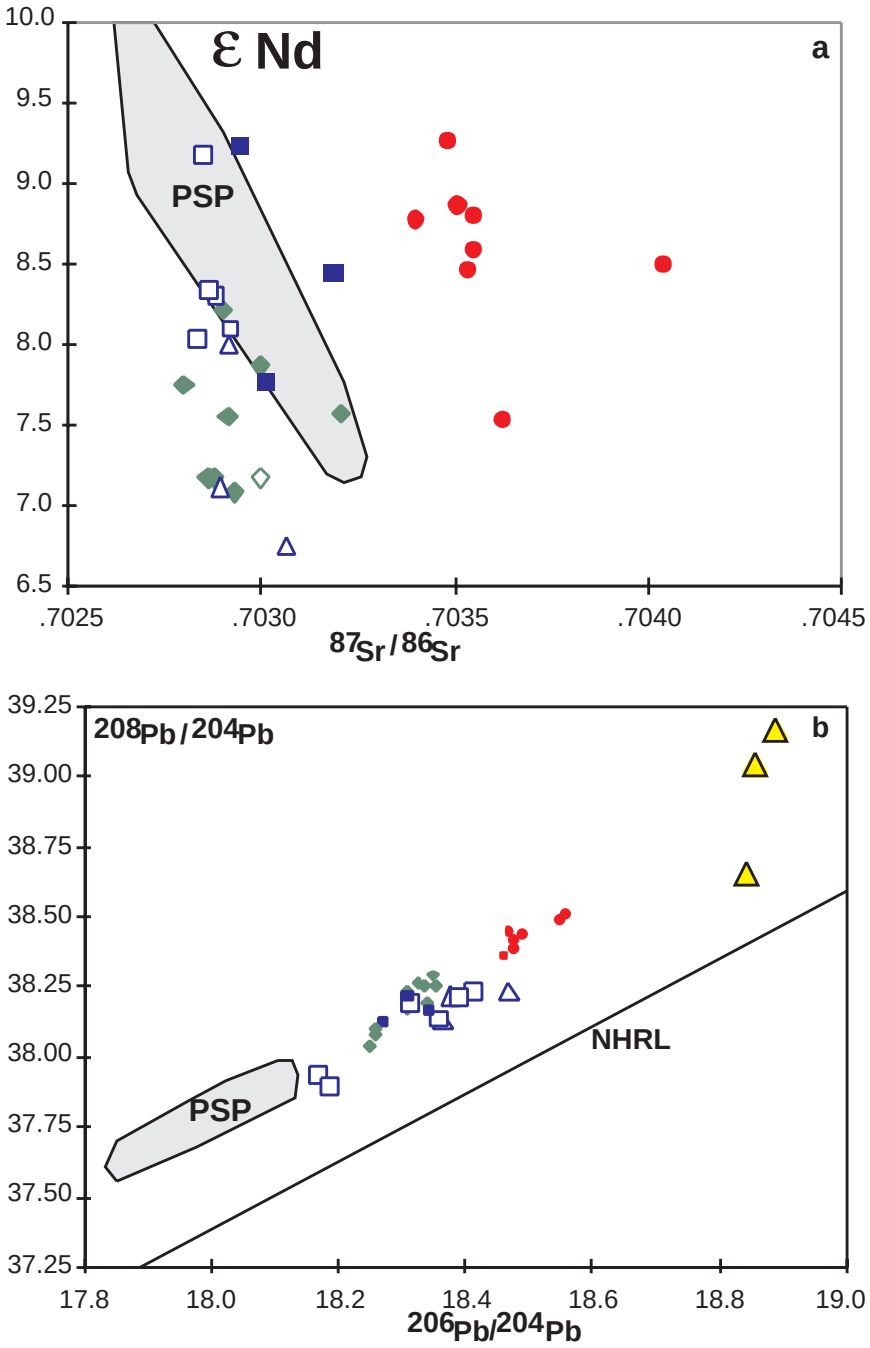

Figure 6. Traditional isotope diagrams show Izu-Bonin volcanic rocks and various mantle and slab end-members from Table 3. On the Pb isotopic diagrams (Figures 8b and 8c) most of the Izu-Bonin volcanic rocks plot above the Northern Hemisphere regression line (NHRL) [*Hart*, 1984] between a field encompassing Shikoku Basin and Philippine Sea Plate (PSP) basalts [*Hickey-Vargas*, 1998] and sediments from the downgoing Pacific Plate.

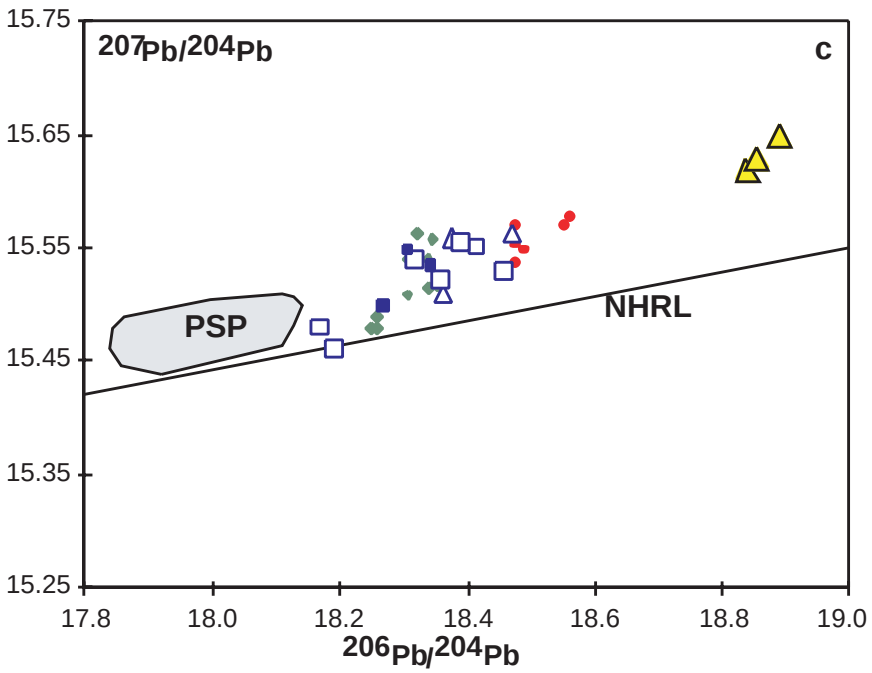

Figure 6. (continued)

non-subduction-related volcanic rocks from the Philippine Sea Plate also plot above the NHRL [*Hickey-Vargas*, 1998].

[23] Trace element ratios between Th, Nb, and Ba are especially instructive because they vary little in nonsubduction oceanic basalts [*Niu and Batiza*, 1997], indicating that the melt/solid partition coefficients for these elements are very similar to each other during mantle melting. Thus the variation in the relative abundance of these elements within and between the Izu-Bonin volcanic suites must result from variations in the subduction component and not from non-slab-related mantle enrichments or melting processes. When Ba/Nb and Th/Nb ratios are considered (Figure 7), Izu-Bonin volcanic rocks plot along two trends, both of which emanate from the oceanic basalt fields and trend in the direction of stronger slab signatures. The two data arrays are characterized by either the VF or the WS suites and, for discussion purposes, are referred to here as the "VF trend" or the "WS trend," respectively. Active rift basalts lie partway along the VF trend, the high K/Na basalts lie at the extreme end of the WS trend, and other extensional volcanics are distributed between the two trends. Clearly, all of the volcanic rocks in the Izu-Bonin arc have been affected by one or more sorts of slab component, including even the WS suite, which has relatively high Nb concentrations and Nb/Zr ratios (Figure 3) [*Hochstaedter et al.*, 2000]. Other trace element ratios that distinguish between the VF and WS trends include, to varying degrees, Pb/Nb, U/Nb, Ba/Th, U/Th, and Pb/Th.

[24] The new Ta results (Table 1 and Figure 3) show that except for the VF, Ta concentrations correlate with Nb concentrations. For all but the VF samples and sample 41-1 from the extensional zone, Nb/Ta ranges from 12.6 to 20, with two modes (13.6 and 17.3), which may be compared with the chondritic ratio of ~17 (*Sun and McDonough*, 1989]. Some of the

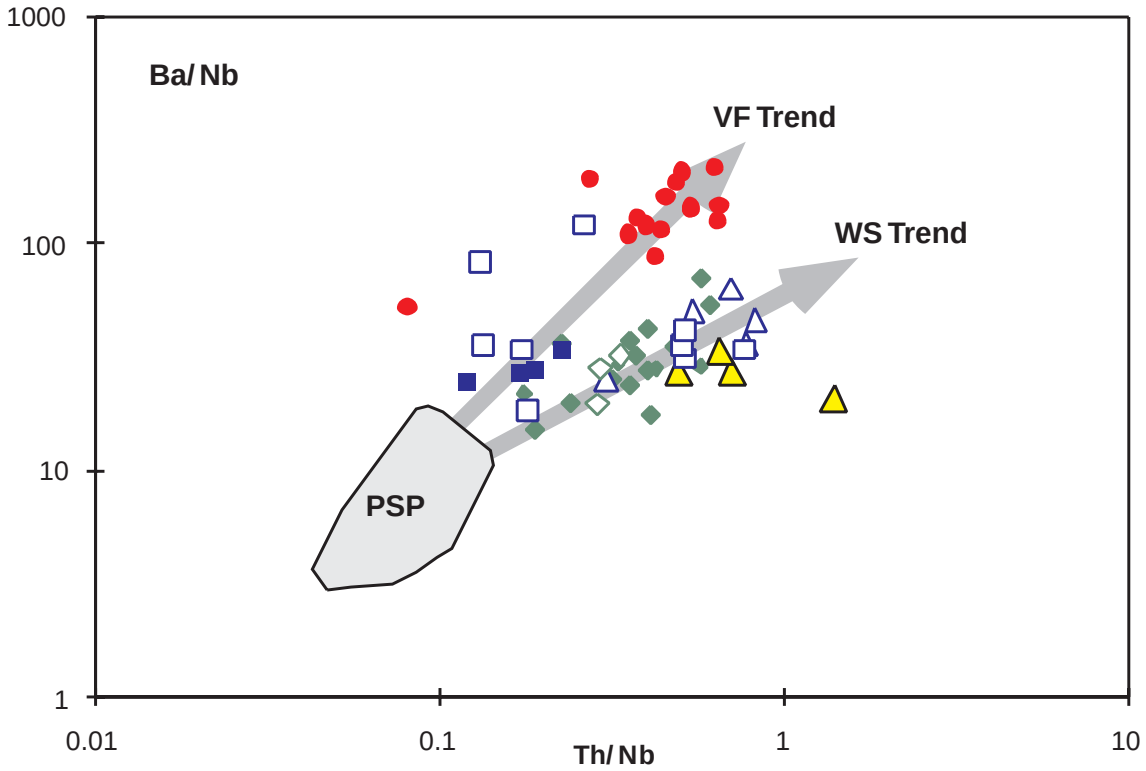

Figure 7. Th/Nb versus Ba/Nb diagram shows two separate trends highlighted by gray arrows, the "VF Trend," which trends to high Ba/Nb and Th/Nb, and the "WS Trend," which trends to moderate Ba/Nb and high Th/Nb. Both trends appear to originate somewhere near the PSP source fields. The chalk sample (Table 2) has a Ba/Nb ratio of ~2000, causing it to plot just off the axis on this diagram; see Figure 9 for the chalk sample.

VF samples and extensional zone sample 41-1, which all contain low amounts of Nb and Ta, have low Nb/Ta ratios (<12.5; Figure 3). These results support the conclusions of *Hochstaedter et al.* [2000] that at least some of the VF is much more depleted than anything else in the arc. The Nb/Zr and Nb/Ta diagrams (Figure 3) show how mantle fertility changes across the arc because of previous melt extraction. This assumes that the percent of melting throughout the arc is high enough (e.g., 15–20%) to preserve source Nb/Zr and Nb/Ta ratios.

5. Discussion

[25] In this section, our goal is to document the characteristics of the slab-derived features that give the Izu-Bonin rocks their distinctive slab signature. In order to do so we distinguish between fertile and residual mantle protoliths, slab-derived components and end-members, and their combination in sources. We will focus first on the mantle protoliths and then on the VF and WS trends. Our approach will be to calculate bulk slab components that could be added to the protoliths to make average WS and VF sources. We will then compare these calculated bulk slab components to typical slab end-members (altered crust, sediments, fluids, and melts) or mixtures between these end-members to see which category most closely resembles the calculated bulk slab components. Finally, we offer a few examples of mixing arrays between source

Table 2. Elemental and Isotopic Analyses for Sediments Outboard of the Izu-Bonin Trench[a]

	Deep Sea Drilling Project Site Section				
	198A-2-2	198A-3-3	195B-3-1	198A	195B-3-1
Sample	103-104	77-76	129-130	5cc	124-125
Lithology	clay	clay	chalk	chert	chert
Nb	14.1	12.5	0.427	0.819	0.147
Zr	141	161	2.61	12.1	0.220
Hf	3.59	4.54	0.144	0.347	0.097
Rb	156	127	5.77	7.26	1.04
Sr	134	167	302	13.3	0.941
Cs	11.6	10.0	0.26	0.500	0.0584
Ba	378	348	621	27.6	3.08
La	92.8	125	4.91	11.8	1.69
Ce	154	178	3.02	9.93	1.11
Pr	28.2	37.1	0.993	2.89	0.493
Nd	123	164	3.92	12.2	2.02
Sm	27.9	36.9	0.773	2.57	0.422
Eu	6.33	8.39	0.281	0.635	0.119
Gd	29.8	40.5	1.03	3.17	0.530
Dy	25.9	36.2	0.948	2.82	0.474
Er	11.5	16.2	0.882	1.71	0.604
Yb	9.66	13.7	0.887	1.60	0.620
Pb	38.6	26.4	0.326	2.51	1.98
Th	9.90	6.12	0.321	0.533	0.203
U	1.32	1.04	0.124	2.88	0.418
$^{143}Nd/^{144}Nd$	0.5120468	0.5120308	0.512286		
ε_{Nd}	−11.5	−11.8	−6.9		
$^{87}Sr/^{86}Sr$	0.71499	0.71230	0.70758	0.71056	0.71030
$^{206}Pb/^{204}Pb$	18.89	18.855	18.84	31.23	
$^{207}Pb/^{204}Pb$	15.65	15.63	15.62	16.51	
$^{208}Pb/^{204}Pb$	39.17	39.05	38.65	39.45	

[a]All elemental concentrations were analyzed by ICP-MS by Hochstaedter from powders donated by R. Stern. Additional analyses of these samples have been published by *Lin* [1992].

compositions and mixtures of the slab-derived end-members.

5.1. What is the Composition of the Presubduction Mantle?

[26] Our estimates of the presubduction mantle composition combine results from *Hochstaedter et al.* [2000] with data from Philippine Sea Plate (PSP) basalts [*Hickey-Vargas*, 1991 ,1998]. PSP basalts are similar to those from the WS, especially in terms of HFSE concentrations and patterns on multielement diagrams (Figure 8). Sr-Nd-Pb isotope ratios also overlap (Figure 6). Low Nb and high Sr and Pb concentrations relative to a smooth pattern in Figure 8a for the WS source are the biggest differences between the two compositions, and even the PSP source has anomalously high K compared to most NMORB or even EMORB. For these reasons we assume that the PSP source is the pristine, prerecent subduction mantle composition that melts beneath the Western Seamounts, although even this source may have experienced earlier slab inputs. Thus we attribute differences between the PSP and WS sources to a slab-

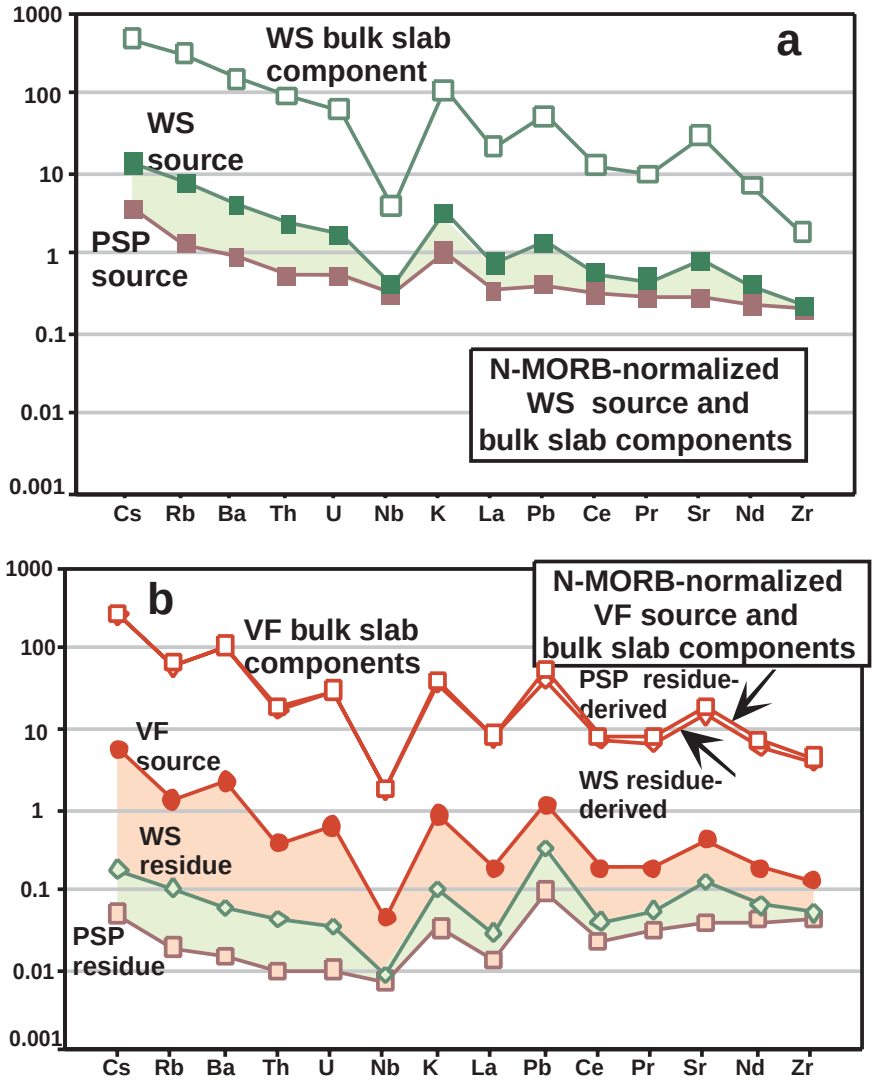

Figure 8. Incompatible element concentrations normalized to normal mid-ocean ridge basalt (NMORB) [*Sun and McDonough*, 1989] are shown. In Figure 8a the shaded region between the PSP and WS sources is assumed to be due to a slab-derived addition into the mantle wedge. This slab input, referred to as the WS bulk slab component, is calculated from mass balance equations assuming 2% slab-derived component mixes with 98% PSP source. The PSP and WS sources are calculated assuming 20% batch melting produces average PSP basalts [from *Hickey-Vargas*, 1991, 1998] and WS lavas. In Figure 8b, VF source uses average VF lavas and also assumes 20% melting. The WS and PSP residues are two possible protoliths for the VF source and are calculated by assuming 4% fractional melt removal from the WS and PSP sources, respectively. The VF bulk slab components are calculated by assuming 2% slab-derived component mixes with 98% of either the WS or PSP residue, as labeled. Figure 8c shows potential slab-derived end-members in the Izu region. Average Izu sediment is a 50:50 mix of clay and chalk from Table 2. Sediment fluid and sediment melt calculated using the partition coefficients from *Johnson and Plank* [1999] closely mimic the shape of average Izu sediment. In contrast, altered oceanic crust (AOC) fluid and sediment fluid calculated using partition coefficients from *Brenan et al.* [1995a, 1995b] differ markedly from the shape of average Izu sediment. All calculated fluids assume that 2% fluid equilibrates with the respective sources. The Johnson and Plank sediment melt assumes 40% melt equilibrates with the source. In Figure 8d the bulk slab components from Figures 8a and 8b are compared with the end-members from Figure 8c. All of the compositions shown here are given in Table 3.

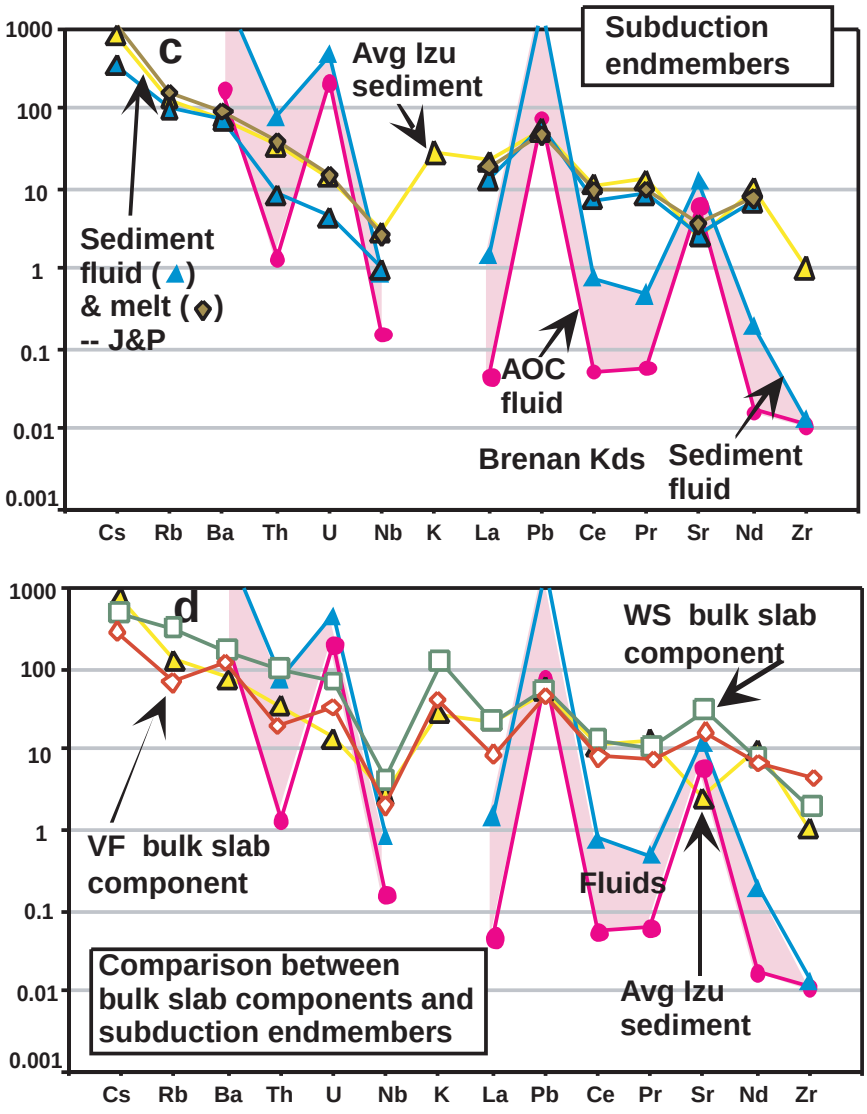

Figure 8. (continued)

derived component added to the WS source. This difference is shown by the shaded region on Figure 8a, which also shows the composition of the requisite WS slab component.

[27] The VF source shown in Figure 8b yields the average VF basalt upon 20% batch melting. Residua after extraction of 4% fractional melt from fertile peridotite provide sources that satisfactorily explain the HFSE characteristics of VF magmas (see *Hochstaedter et al.* [2000] for details). The 4% melt extraction differs from the 4.5% figure used by *Hochstaedter et al.* [2000] because the previous study used a WS source that would produce the most enriched WS composition (in terms of mantle-derived components), whereas in this paper we use a WS source that will produce average WS compositions. Two VF source compositions are shown on Figure 8b. They are residues from the WS and

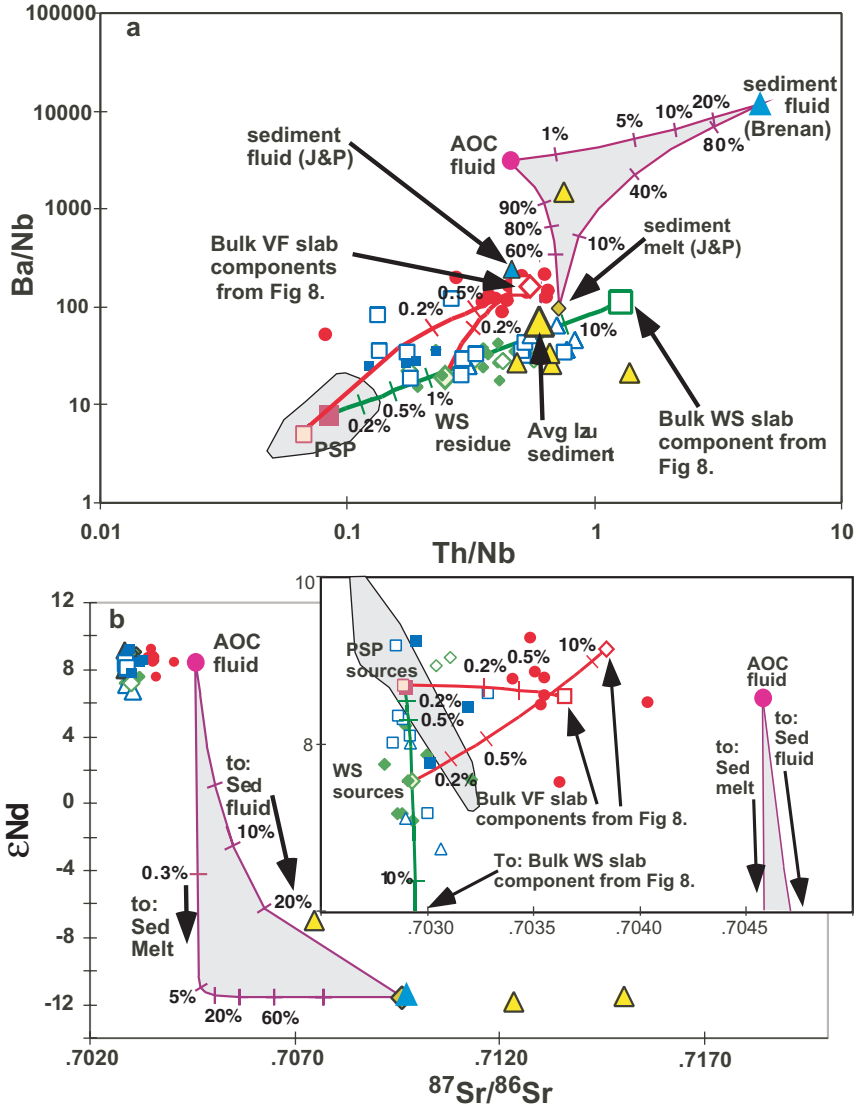

Figure 9. (a and b) Volcanic rock compositions, end-members, and bulk slab components from Figure 8 and Table 3 are shown. The shaded regions encompass PSP basalts [from *Hickey-Vargas*, 1991, 1998] and mixtures between the slab end-members. Labeled tick marks on the sides of the shaded slab end-members field give an indication of the proportion of the end-members in the mixture. The red and green lines show mass balance mixing lines for the VF and WS, respectively, between mantle compositions and calculated bulk slab components from Figure 8 and Table 3; the green line extends from the fertile PSP source to the bulk WS slab component. Symbols are as from Figure 1. The dark red solid square is the fertile PSP source, and the lighter red solid square, which plots at slightly lower Th/Nb values, is its residue after melt extraction. The residual WS source is labeled; the fertile WS source is not shown. (c) Nd isotopes and Tn/Nd show how average Izu sediment, sediment melt, or sediment fluid, as calculated using the *Johnson and Plank* [1999] partition coefficients, all lack sufficiently high Th/Nd to explain the high Th/Nd ratios of the WS trend as shown by the subvertical gray arrow. A mixture between AOC fluid and sediment fluid, as calculated using the *Brenan et al.* [1995a, 1995b] partition coefficients, can explain the WS trend, as shown by the subhorizontal gray arrow.

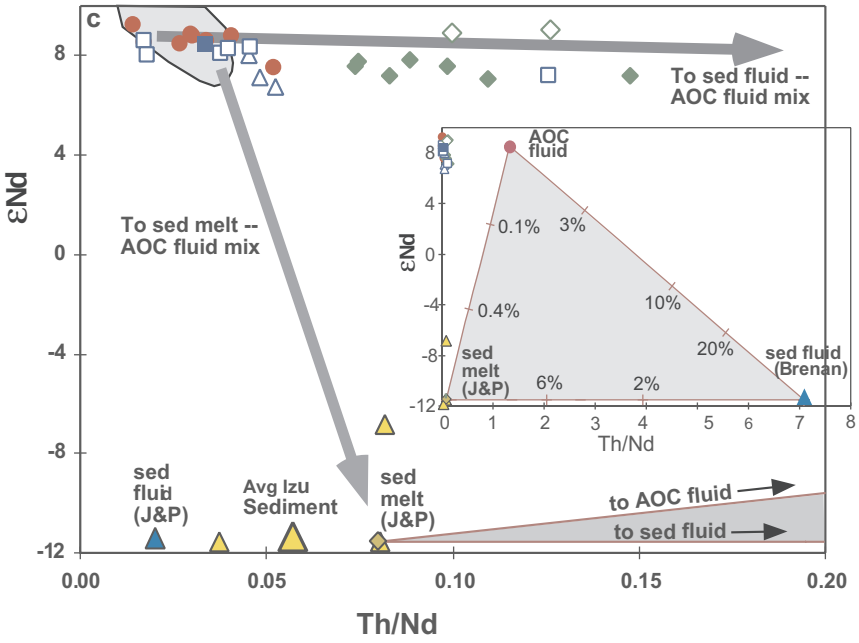

Figure 9. (continued)

PSP sources. The difference between either residue and the VF source must be produced by influx of a slab-derived component at the VF. These differences are shown by shaded regions on Figure 8b, which also shows the compositions of the requisite VF slab components.

[28] Different VF source protoliths (i.e., WS versus PSP residues) lead to different inferences about mantle wedge dynamics. If a residual PSP source is used, then the slab component that metasomatized the mantle wedge at the WS source region did not affect the mantle that later produced the VF suite. For example, the slab-derived component may have mixed with WS melts but not the mantle. In contrast, if the residual WS source is used, it implies that the WS source mantle is first metasomatized by one slab component, then is depleted by melt extraction, then remelts beneath the VF when fluxed by another slab component.

[29] The ambiguity between the two potential sources is illustrated in Figure 9 using Ba/Nb, Th/Nb, and ε_{Nd} ratios. Similarity of Th/Nb in both VF and WS suites suggests that the VF protolith was the WS residue, whereas differences in ε_{Nd} suggest that the VF protolith was the PSP residue. If the VF source is also the WS residue, then the high Th/Nb of the VF may be attributed to a subduction-related addition of Th to the WS source. However, because the ε_{Nd} of the WS source is significantly lower than that of the VF, the VF subduction component would then have to raise the ε_{Nd} of the WS residue to produce VF magmas with high ε_{Nd}, or the differences in ε_{Nd} between the VF and WS requires presubduction heterogeneity in the mantle. In contrast, if the VF source is the PSP residue, then Th must be added at both the VF and WS, while ε_{Nd} remains unchanged during addition of the subduction component.

5.2. *Bulk Slab Components in the Izu-Bonin Arc*

[30] The bulk slab components shown in Figures 8a and 8b are calculated by using mass balance equations assuming that (1) the difference between the presubduction sources (i.e.,

Table 3. End-Member Compositions Used in Models

	Mantle Sources					Bulk Slab Components		
	PSP Source[a]	PSP Residue[b]	WS Source[c]	WS Residue[d]	VF Source[e]	WS[f]	VF (PSP Res)[g]	VF (WS Res)[h]
Nb	0.742	0.017	0.910	0.021	0.102	9.12	4.28	4.09
Zr	15.0	3.25	17.4	3.79	9.61	137	321	295
Sr	24.6	3.52	76.6	11.0	37.6	2626	1706	1341
K	627	19.6	1969	61.5	501	67721	24096	22043
Cs	0.027	0.00035	0.0949	0.00124	0.0390	3.44	1.93	1.89
Rb	0.754	0.0105	4.30	0.0601	0.741	178	36.5	34.1
Ba	5.90	0.0878	25.7	0.382	14.2	994	705	691
La	0.871	0.0327	1.92	0.0722	0.457	53.4	21.3	19.3
Ce	2.42	0.171	4.25	0.301	1.37	94.0	60.2	53.9
Pr	0.361	0.0427	0.610	0.0722	0.243	12.8	10.1	8.61
Nd	1.73	0.291	2.76	0.464	1.35	53.3	53.1	44.7
Sm	0.550	0.145	0.708	0.186	0.450	8.42	15.4	13.4
Eu	0.198	0.069	0.232	0.081	0.163	1.91	4.76	4.18
Gd	0.743	0.312	0.824	0.346	0.646	4.79	17.0	15.3
Dy	0.932	0.531	0.836	0.476	0.776		12.8	15.5
Er	0.592	0.374	0.492	0.311	0.516		7.50	10.6
Yb	0.628	0.446	0.521	0.370	0.565		6.38	10.1
Pb	0.126	0.0286	0.438	0.0991	0.342	15.7	15.7	12.3
Th	0.0620	0.00110	0.288	0.00509	0.0463	11.4	2.26	2.06
U	0.0246	0.000460	0.086	0.00161	0.0295	3.11	1.45	1.40
$^{87}Sr/^{86}Sr$	0.702897	0.702897	0.702935	0.702935	0.703580	0.702952	0.703653	0.703844
$^{144}Nd/^{143}Nd$	0.513085	0.513085	0.513025	0.513025	0.513080	0.512930	0.513077	0.513106
ε_{Nd}	8.7	8.7	7.5	7.5	8.6	5.7	8.6	9.1
$^{206}Pb/^{204}Pb$	17.98	17.98	18.31	18.31	18.50	18.44	18.54	18.57
$^{207}Pb/^{204}Pb$	15.47	15.47	15.52	15.52	15.56	15.54	15.56	15.57
$^{208}Pb/^{204}Pb$	37.79	37.79	38.20	38.20	38.43	38.36	38.49	38.52

Table 3. (continued)

	Slab End-Members						Residual Slab End-Members[i]			
	Avg Izu Sed[j]	Sed Fluid 1[k]	Sed Fluid 2[l]	Sed Melt[m]	AOC[n]	AOC Fluid[o]	Avg Izu Sed	Sed Fluid	AOC	AOC Fluid
Nb	6.86	2.05	2.32	6.09	1.22	0.364	6.96	2.08	1.24	0.369
Zr	76.7	0.978			66.5	0.848	78.2	0.998	67.8	0.86508
Sr	226	1097	248	321	115	558	209	1011	106	514
K	16833				4648					
Cs	5.55		2.40	7.72	0.153					
Rb	73.6		56.1	88.5	9.58					
Ba	492	24332	474	579	22.6	1117	5.60	277	0.257	12.7
La	57.0		33.8	47.3	1.84					
Ce	84.6	5.79	54.6	69.9	6.01	0.411	86.21	5.8958	6.1243	0.419
Pr	16.8		11.0	13.1	1.17					
Nd	73.6	1.39	51.4	55.8	6.62	0.125	75.1	1.42	6.75	0.128
Sm	16.6	0.172	10.4	12.2	2.50	0.0259	16.9	0.175	2.55	0.0264
Eu	3.82				0.91					
Gd	18.1				3.65					
Dy	16.0				4.4					
Er	7.35				2.77					
Yb	6.28	0.0482	1.74	4.46	2.69	0.021	6.41	0.0492	2.74	0.0211
Pb	16.4	550.5	17.4	14.0	0.7	23.49	5.5053	185	0.235	7.88
Th	4.165	9.876	1.02	4.46	0.07	0.166	4.05	9.60	0.0680	0.161
U	0.652	21.88	0.22	0.68	0.3	10.07	0.219	7.34	0.101	3.38
$^{87}Sr/^{86}Sr$	0.709597	0.709597	0.709597	0.709597	0.704575	0.704575	0.709597	0.709149	0.704575	0.704575
$^{144}Nd/^{143}Nd$	0.512045	0.512045	0.512045	0.512045	0.513077	0.513077	0.512045	0.512047	0.513077	0.513077
ε_{Nd}	-11.6	-11.6	-11.6	-11.6	8.6	8.6	-11.6	-11.5	8.6	8.6
$^{206}Pb/^{204}Pb$	18.87	18.87	18.87	18.87	18.3	18.3	18.87	18.87	18.30	18.30
$^{207}Pb/^{204}Pb$	15.64	15.64	15.64	15.64	15.46	15.46	15.64	15.64	15.46	15.46
$^{208}Pb/^{204}Pb$	39.11	39.11	39.11	39.11	37.7	37.7	39.11	39.11	37.70	37.70

the protoliths) and the average source compositions of the VF and WS suites is due to a slab component and(2) the slab-derived component represents 2% of the metasomatized source. (For comparison, *Ayers* [1998] calculated 17% and *Taylor and Nesbitt* [1998] calculated 0.5–1.0% for the slab contribution at volcanic fronts.) For the WS suite an average PSP source is used as the protolith; for the VF suite both PSP and WS residues were used, although results are very similar because even 2% of the slab component swamps both of them. Bulk slab components for the Izu-Bonin arc are given in Table 3 and shown in Figures 8 and 9.

[31] The bulk slab components required for the WS and VF suites differ. The WS bulk slab component is enriched in all non-HFSE elements with solid/melt partition coefficients lower than Zr (Figure 8a). It has small positive spikes in Sr, Pb, and K. In contrast, the VF bulk slab component is more variable; it has elevated Sr, Pb, K, U, and Ba concentrations but relatively low concentrations of Th and light REE. This result is one of the main conclusions of this study: the bulk slab component that metasomatizes the WS source is different from the one that metasomatizes the VF source. This difference is manifested mainly in the ratios of the elements Cs, Rb, Ba, Th, and U.

Notes to Table 3:

[a]Mantle source calculated from an average of 16 basalts from the Shikoku Basin (Sites 442B, 443, and 444A), the West Philippine Basin (Suite 291and 447A), and the Parece Vela Basin (Site 449 and 450). A wide compositional variety of basalts were included in the average so as to incorporate as much of the inherent heterogeneity within the Philippine Sea Plate (PSP) as possible. Only those basalts with $^{206}Pb/^{204}Pb$ <18.2 were included so that the HIMU type of heterogeneity would be excluded from the average. This assumes 20% batch melting produced the average PSP basalt. Data are from *Hickey-Vargas* [1991, 1998].

[b]Residue from the average PSP source after 4% fractional melt extraction following the techniques of *Hochstaedter et al.* [2000].

[c]Mantle source calculated from an average of basalt and andesite data from the Western Seamounts.This assumes 20% batch melting produced the average parental basalt.

[d]Residue from the average WS after 4% fractional melt extraction following the techniques of *Hochstaedter et al.* [2000].

[e]Mantle source calculated from an average of basalt and andesite data from the Volcanic Front. This assumes 20% batch melting produced the average parental basalt.

[f]WS bulk slab component is calculated by assuming that the difference between the PSP source and WS source is produced by the addition of 2% slab component.

[g]VF bulk slab component is calculated by assuming that the difference between the PSP residue and VF source is produced by the addition of 2% slab component.

[h]VF bulk slab component is calculated by assuming that the difference between the WS residue and VF source is produced by the addition of 2% slab component.

[i]Residual slab components represent sediments and AOC after 2% fluids have been removed from them, using fluid/solid partition coefficients from *Brenan et al.* [1995a, 1995b]. The columns labeled "fluid" are the fluids that could then be extracted from these residual compositions, again assuming the same fluid/solid partition coefficients from *Brenan et al.* [1995a, 1995b].

[j]This is the average Izu sediment with 50% clay and 50% chalk from Table 2.

[k]Fluid released as sediments dehydrate in the subduction zone. This assumes 2% fluid in equilibrium with the sediments and fluid/solid partition coefficients (gt:cpx:rut = 59.5:39.5:1) from *Brenan et al.* [1995a, 1995b].

[l]Fluid released as sediments dehydrate in the subduction zone. This assumes 2% fluid in equilibrium with the sediments and fluid/solid partition coefficients from *Johnson and Plank* [1999].

[m]Sed melt is sediment melt. This assumes 40% melt in equilibrium with the sediments and melt/solid partition coefficients from *Johnson and Plank* [1999].

[n]Altered oceanic crust (AOC) is from *Staudigel et al.* [1996] and the Geochemical Earth Reference Mode (GERM) Web page (http://earthref.org/GERM/). This was not used as a direct slab end-member.

[o]Fluid released as AOC dehydrates in the subduction zone. This assumes 2% fluid in equilibrium with AOC and the fluid/solid partition coefficients (gt:cpx:rut = 59.5:39.5:1) from *Brenan et al.* [1995a, 1995b].

5.3. End-Members From the Subducting Slab

[32] End-member refers here to a combination of slab source and transfer agent. We will consider three end-members: fluid derived from average Izu sediment (''sediment fluid''), fluid derived from altered oceanic crust (''AOC fluid''), and melt derived from average Izu sediment melt (''sediment melt'') (Figure 8c and Table 3). Our average Izu sediment is an equal weighting of pelagic chalk and clay because they are roughly in equal proportions in ODP Site 1149 in the Nadeshda Basin outboard of the Izu arc [*Plank et al.*, 1999]. The abundant chert is considered a dilutant for these elements and is ignored. Average Izu sediment refers specifically to a mixture between clay and chalk not sediment fluid or sediment melt. For AOC we used a global average compiled by *Staudigel* [1996] (see the Geochemical Earth Reference Model (GERM) Web page, http://earthref.org/GERM/). The AOC fluids were calculated using standard mass balance equations with the AOC as the starting composition, *Brenan et al.*'s [1995a, 1995b] rutile-eclogite/fluid partition coefficients, and 2% fluids equilibrating with the downgoing eclogite. (For comparison, *Ayers* [1998] used similar partition coefficient D values but 20% fluids.) The sediment fluids were calculated in the same way, even though *Brenan et al.*'s [1994, 1995a, 1995b] partition coefficients may not be as applicable to a sediment composition. We also evaluated sediment fluid and sediment melt compositions calculated using *Johnson and Plank*'s [1999] bulk partition coefficients. The difference between the two calculated sediment fluids illustrates current uncertainties. The results for sediment melt assume 40% melting appropriate for the 900°C D values from *Johnson and Plank* [1999]. Fluid concentrations were not calculated for all elements because eclogite/fluid partition coefficients are available for only certain elements.

5.4. Comparison of Bulk Slab Components With Subduction End-Members

[33] In this section we compare the calculated bulk subduction component for both the VF and WS suites to the end-members or mixtures between the end-members. We use the trace element patterns in Figure 8 as a starting point and then test the results using plots of isotope and trace element ratios. Figure 9 shows the bulk slab compositions from Figure 8c along with fields that encompass mixtures between the slab-derived end-members, including sediment melt, sediment fluid, and AOC fluid.

5.4.1. Identity of the VF slab component

[34] On the basis of the trace element patterns on Figure 8 and the position of the bulk slab components on Figure 9 the VF slab component appears most similar to a slab-derived hydrous fluid. Fluids are a better choice than either average Izu sediment or sediment melt because of the pronounced spikes in Ba, U, K, Pb, and Sr relative to Th and La in the slab component calculated for the VF (Figure 8). However, using the values we have adopted, Ba/Nb ratios (and U/Nb, Pb/Nb, and Sr/Nb) in the VF are too low to be explained quantitatively by a fluid-dominated transfer agent. The elevated Sr and Pb isotope ratios of the VF relative to their Nd isotopic composition also indicate the importance of hydrous fluids at the VF because Pb and Sr but not Nd are considered fluid-mobile elements.

[35] From these diagrams alone it is unclear whether the fluids are derived from sediments or AOC. However, Pb isotopes provide strong evidence that the source of the fluids is a mixture of average Izu sediment and AOC (Figure 10a). The Pb isotopic composition of Pacific-type AOC differs substantially from

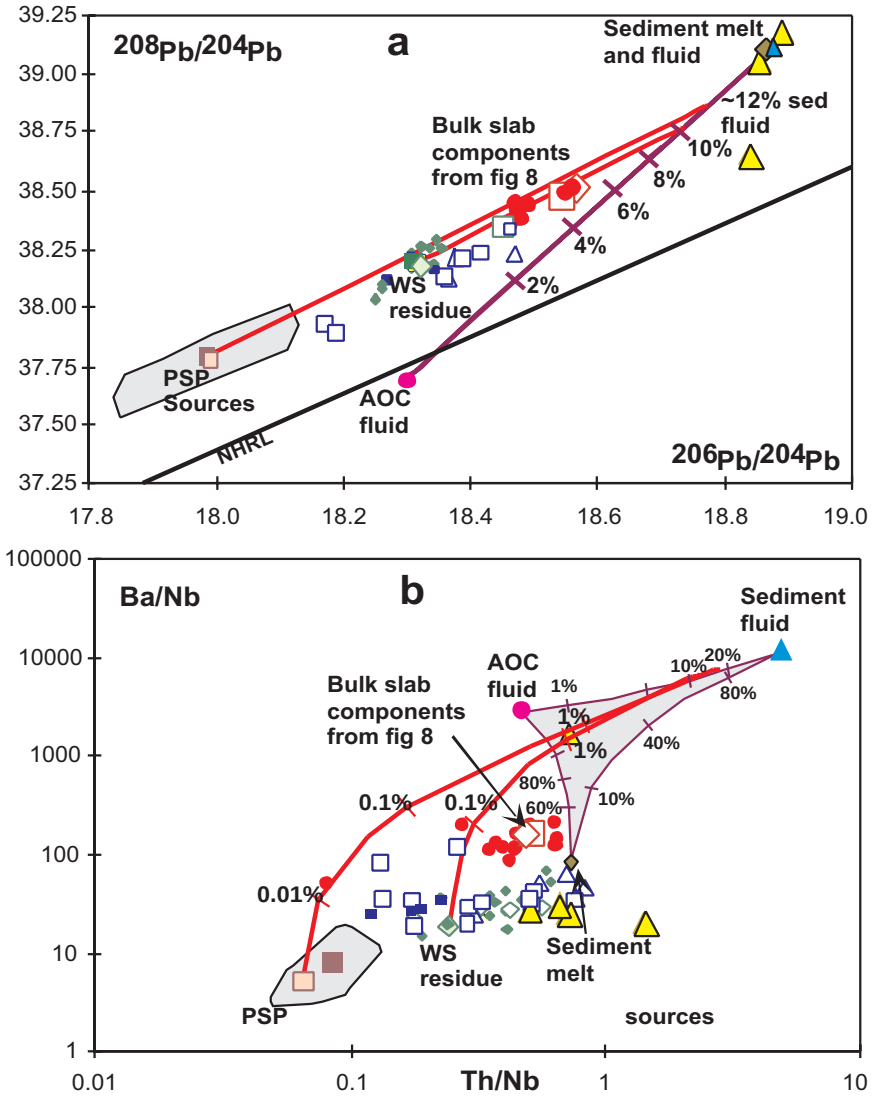

Figure 10. These diagrams show mixing curves that could potentially explain the VF trend. The mixing curves emanate from the PSP or WS residues (from Figure 8 and Table 3) and trend toward a mixture of sediment fluids and AOC fluids. The proportions of sediment fluids and AOC fluids in the mixture are constrained by the Pb isotopes (Figure 10a) as 12:88 sediment:AOC. In Figures 10b–10d the PSP residue is more appropriate for a VF protolith in the diagrams involving Nd isotopes, but the WS residue is more appropriate for a VF protolith in the Th/Nb versus Ba/Nb diagram. The mixing lines in these diagrams also trend toward the same 12:88 sediment:AOC fluid mixture. Symbols are as from Figure 1.

both average Izu sediments and the Indian-type PSP mantle protolith, which offers a way to distinguish between the potential fluid sources. The VF and WS suites plot along a straight line between a PSP source and a mixing line that connects average Izu sediments and AOC. The proportions of the end-members of the AOC-sediment mixing line depend upon the transfer agent (and subsequent element concentrations) from the sediment and the clay/chalk ratio of

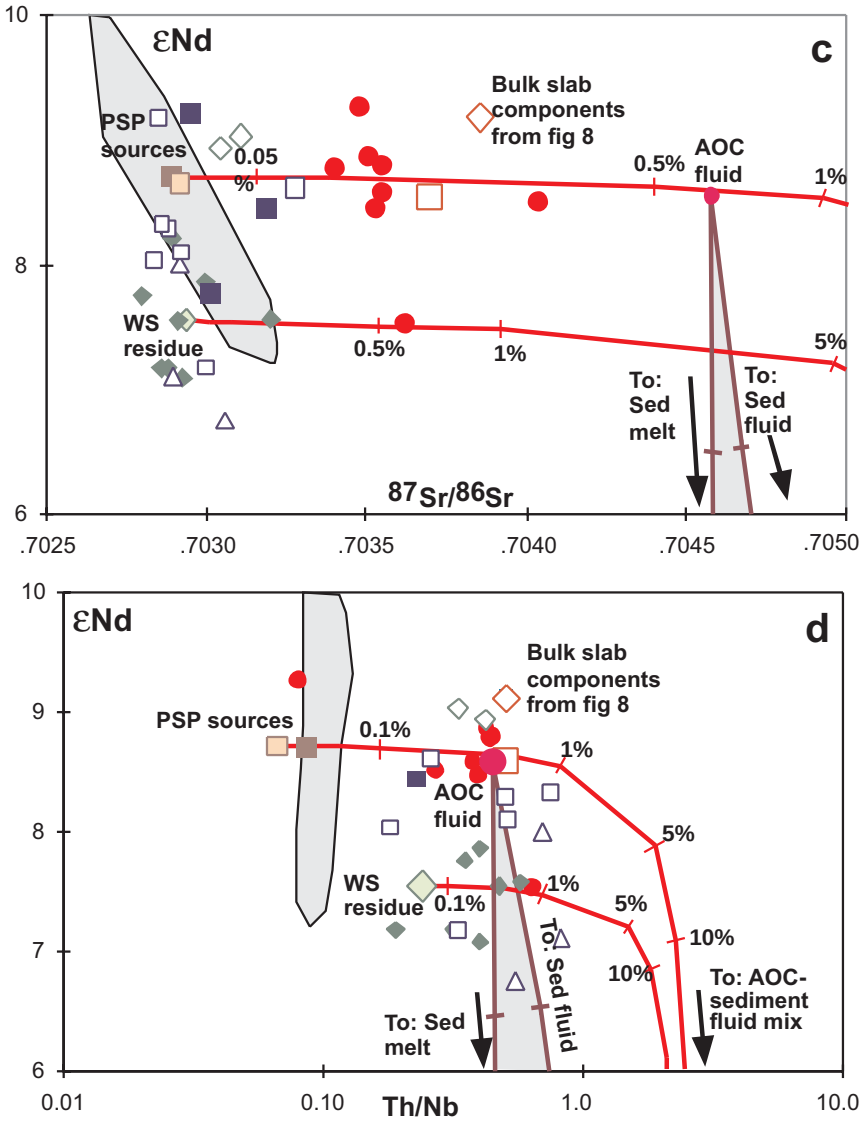

Figure 10. (continued)

the sediment. The AOC-derived component is assumed to be a hydrous fluid since old, cold crust probably does not melt beneath the VF. If the sediment transfer agent is also a fluid, then the resulting fluid is ~12% sediment-derived and about 88% AOC-derived. For comparison, using similar logic, *Taylor and Nesbitt* [1998] concluded that the mantle metasomatizing fluid at the Izu volcanic front was 98% from AOC and 2% from sediment.

[36] There is no evidence for the involvement of sediment melt at the Izu volcanic front. Adding sediment melt to a mixture of AOC fluid and sediment fluid (much less replacing sediment fluid with sediment melt) decreases the match with the VF trend and the bulk VF slab component in Figures 7–10. Furthermore, if sediment melt were involved, lower ε_{Nd} values would result because sediment melts are richer in Nd with low ε_{Nd} values (Figure 9).

[37] Having established that at the VF, PCS or WS residue is metasomatized by a fluid derived from both AOC and sediment, we now explore the quantitative implications of the Pb isotope data. Figures 10b–10d apply the mixing proportions indicated by Pb isotopes (Figure 10a) to the elemental and isotopic systematics shown in Figure 9. Two mixing lines are shown in each plot. One illustrates the effects of the fluid mixture added to the PSP residue, the other shows the effects of the fluid mixture added to the WS residue. In addition, the effects of a different set of partition coefficients relevant to sediment fluid (*Johnson and Plank*, 1999) are shown for comparison.

[38] On ε_{Nd} versus $^{87}Sr/^{86}Sr$ or Th/Nb diagrams the mixing line emanating from the PSP residue passes through the VF trend (Figures 10c and 10d) using *Brenan at al.*'s [1995a, 1995b] partition coefficients. However, no quantitative model simultaneously explains the behavior of both highly fluid-mobile elements, such as Ba and U, and also less fluid-mobile elements, such as Th (Figure 10b). Mass balance mixing arrays that connect the PSP residue to slab-derived fluids are strongly curved on the Ba/Nb versus Th/Nb diagram of Figure 10b, causing them to miss the VF field. That is, Th is more mobile at the VF than is explicable by even *Brenan et al.*'s [1995a, 1995b] fluid *D* values, much less *Johnson and Plank*'s [1999], or else the PSP residue is inappropriate as a VF source. Quantitative mixing arrays using the WS residue fare slightly better on the Th/Nb versus Ba/Nb diagram (Figure 10b). Essentially, because the Th/Nb ratio in the WS residue source is elevated as a result of preferential Nb loss during prior melt extraction, addition of slab-derived fluids to WS residue would increase the Ba/Nb and U/Nb and leave Th/Nb relatively unchanged. Mixing arrays between the slab-derived fluids and the WS residue would still have the same concave shape but trend closer to the VF field (Figure 10b). However, ε_{Nd} in the WS residue is too low for the VF (Figures 10c and 10d).

[39] In summary, we conclude that the subduction component that metasomatizes the VF source region is a fluid derived from both AOC and sediments. We infer that 88% of this fluid is derived from AOC, the balance coming from a 1:1 mix of pelagic clay and chalk diluted by chert. We reach this conclusion based on the relative enrichments of the fluid-mobile elements Ba, Sr, Pb, and U in the bulk VF slab component on Figure 8 and the placement of this calculated slab component on elemental and isotopic variation diagrams (Figures 9 and 10), even though we cannot uniquely and quantitatively explain the VF trend using mixtures of slab end-members listed in Table 3.

5.4.2. Identity of the WS slab component

[40] The identity of the slab component for the WS is more difficult to determine, and it may not even be a recent "slab component." On multielement diagrams (Figure 8) the patterns of both the WS source and its calculated slab component are flatter and less variable than for the VF suite. Specifically, Rb, Th, and LREE are less depleted relative to nearby elements than in the VF suite. Nb is still depleted relative to adjacent elements but not as much as in the VF suite and not at all relative to the heavy REE or even Zr. The stronger enrichments in Th and LREE make for an overall smoother pattern (Figure 8) and could suggest the involvement of sediment melt rather than a sediment fluid as the mass transfer agent. The merit of this suggestion is illustrated in Figure 9a, where the sediment melt composition lies near the WS trend and the bulk WS slab component.

[41] Indeed, the WS trend shares some features attributed to sediment melts in other arcs [e.g.,

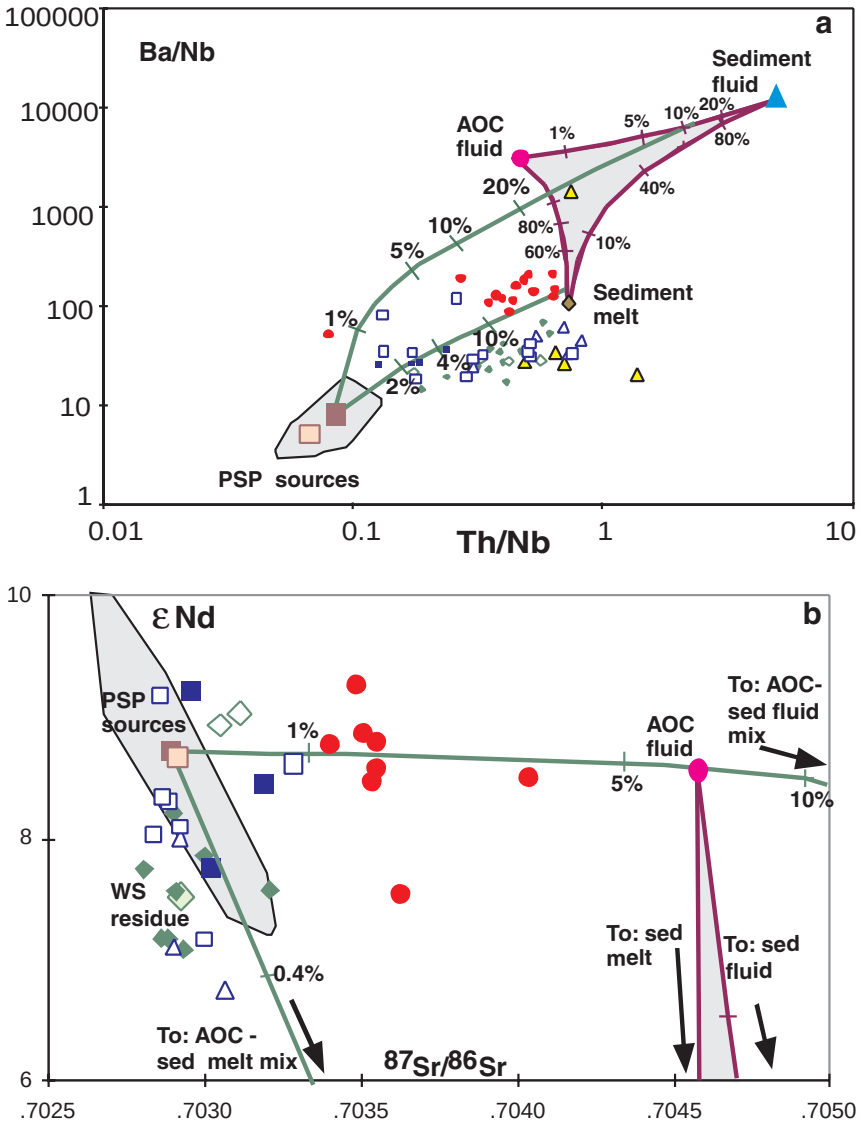

Figure 11. These diagrams all show mixing curves that could potentially explain the WS trend. The mixing curves emanate from the PSP source and trend toward mixtures of either Izu sediment melt and AOC fluid in the proportions 77:23 sediment melt:AOC fluid or sediment fluid and AOC fluid in the proportions 12:88 sediment:AOC (all end-members from Figure 8 and Table 3). As in Figure 10, the proportions of the end-members in the slab component mixture are constrained by Pb isotopes. The mixture involving Izu sediment melt explains the data adequately on Figures 11a and 11b, but the mixture involving sediment fluid is better on Figure 11c. A single mixture of these slab end-members cannot adequately explain all of the data. Symbols are as from Figure 1.

Elliott et al., 1997; *Class et al.*, 2000]. These features include the smoother element diagrams referred to above, lower ε_{Nd}, and higher Th/Nd ratios. However, unlike these other arc suites, in Izu these features are accompanied by lower $^{87}Sr/^{86}Sr$ and $^{206}Pb/^{204}Pb$ ratios, ε_{Nd} does not correlate with Ce anomalies in REE patterns or Th/Nb ratios, and quantitative mod-

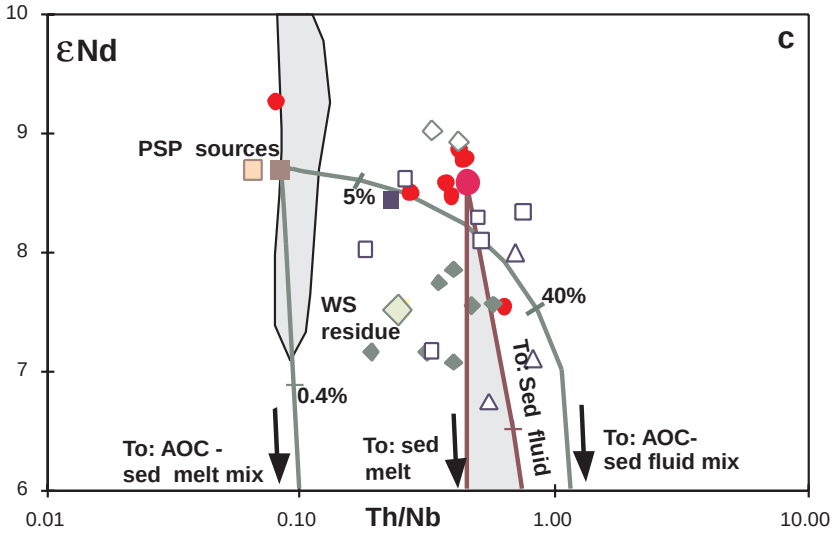

Figure 11. (continued)

els of sediment melt addition fail, as discussed below.

[42] In Pb isotopic space, the WS suite lies along the same array as does the VF suite materials derived from sediment and AOC. Pb isotopic systematics constrain the mixture in the following ways, which are essentially the same as for the VF. If the mixture is entirely fluid, then ~12% of the mixture is sediment-derived. However, if the mixture is AOC fluid plus sediment melt, then ~77% of the mixture is sediment melt. The implications of these proportions are explored in Figure 11.

[43] WS rocks have lower $^{87}Sr/^{86}Sr$, ε_{Nd}, and $^{206}Pb/^{204}Pb$ ratios than the VF suite. These isotope ratios help distinguish the transfer agent involved in the WS subduction component. The mixing trend between the PSP source and AOC-sediment fluid combination miss the WS data array in all element and isotope ratios regardless of which fluid *D* values are used. This trend becomes very enriched in $^{87}Sr/^{86}Sr$ and $^{206}Pb/^{204}Pb$ before the ε_{Nd} decreases to the levels of the WS suite. This conclusion is strengthened by our discovery of lower $^{87}Sr/^{86}Sr$ ratios than previously reported for the WS. Any involvement of fluid as a transfer agent brings strong enrichments of Ba, U, Sr, and other fluid-mobile elements, which cause concave down mixing curves on the Ba/Nb versus Th/Nb diagram (Figure 11a). These mixing curves bypass the WS trend even more than the VF trend.

[44] The mixing line to the sediment melt plus AOC fluid combination trends very close to the WS suite on the Sr-Nd isotope diagram and on the Ba/Nb-Th/Nb trace element diagram (Figure 11). On other diagrams, however, the mixing line for the sediment melt-AOC fluid misses the WS suite altogether. On the Th/Nb-ε_{Nd} diagram (Figure 11c), for example, the sediment melt-AOC fluid mixing trend does not have high enough Th/Nb to pass through the WS array. The moderate Th and high Nd concentrations in this mixture cause the mixing line to drop in ε_{Nd} more substantially than it increases in Th/Nb. Even WS samples with elevated Th do not have the low ε_{Nd} required by influx of sediment melt.

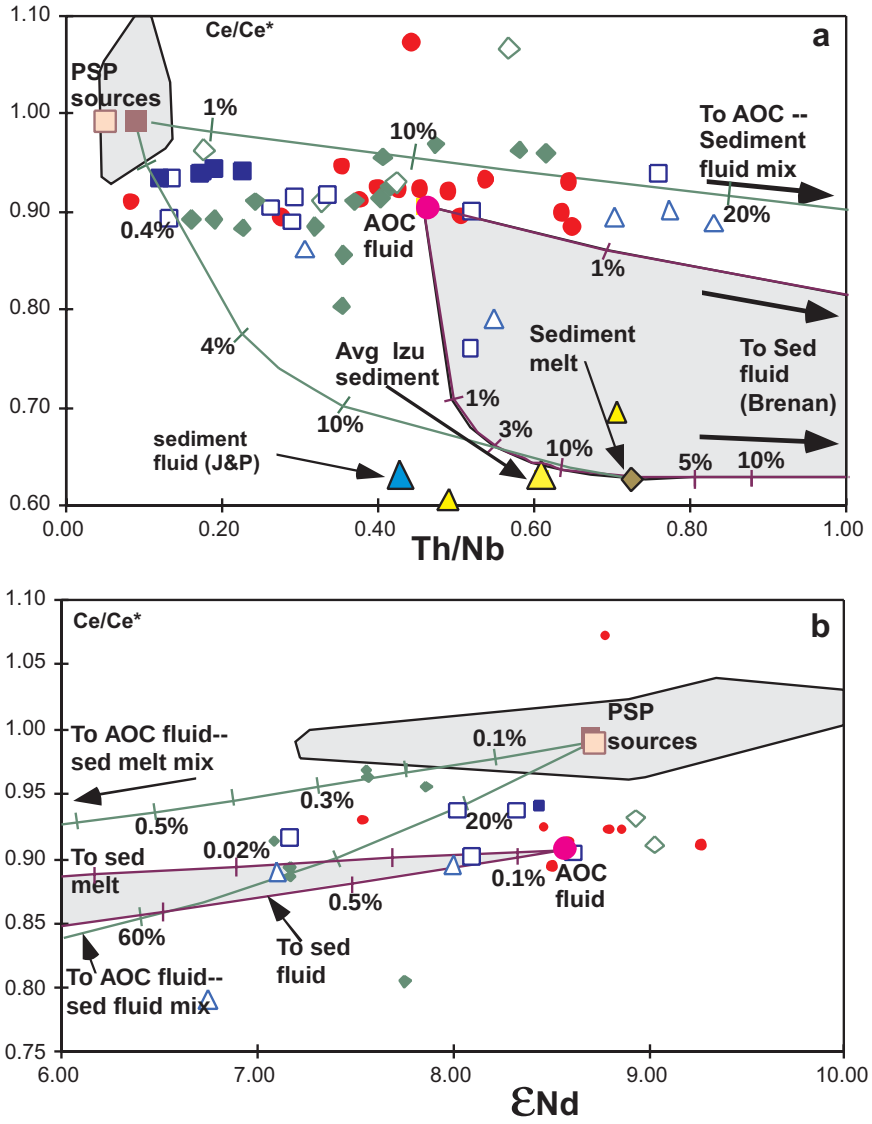

Figure 12. Ce/Ce* is a sediment indicator because some oceanic sediments contain negative Ce anomalies. Ce* is calculated by calculating the average of chondrite normalized La and Pr. Sediments analyzed for this study contain Ce/Ce* between 0.2 and 0.7 (Table 2), and the value for average Izu sediment is 0.63 (Table 3). Ce/Ce* values for Izu-Bonin volcanic rock average ~0.92 and do not strongly correlate with Th/Nb or ε_{Nd}, the other indicators of sediment contribution, indicating that average Izu sediment or associated melts do not play an important role in the genesis of Izu-Bonin volcanic rocks. The mixing lines are as in Figure 12. They emanate from the PSP source and trend toward mixtures of either Izu sediment melt and AOC fluid in the proportions 77:23 sediment melt:AOC fluid or sediment fluid and AOC fluid in the proportions 12:88 sediment:AOC (all end-members from Figure 8 and Table 3). Symbols are as from Figure 1.

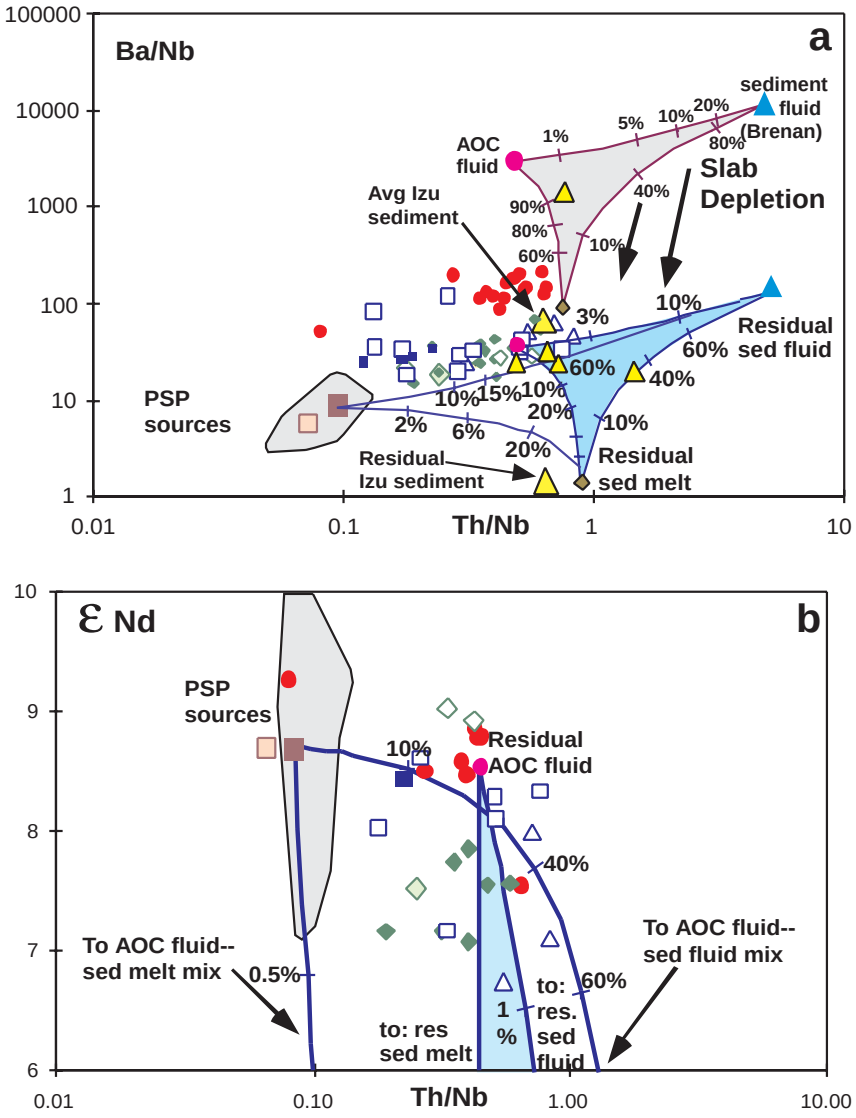

Figure 13. The "residual slab" hypothesis to explain the WS trend is shown. Slab dehydration during subduction will cause the composition of the slab to become depleted in fluid-mobile elements. Residual sediment and residual AOC are calculated by assuming 2% fluid leaves the slab beneath the VF and using the partition coefficients of *Brenan et al.* [1995a, 1995b]. Mixing lines emanate from the PSP source and trend toward either mixtures of fluids derived from residual Izu sediments and residual AOC (sediment fluid:AOC fluid is 12:88) or mixtures of residual sediment melt and residual AOC fluid (sediment melt:AOC fluid is 77:23). The mixing line involving the residual fluid mixture trends through or close to the WS data array on Figures 13a and 13b. The mixing line involving residual Izu sediment melt does not trend through or close to the WS data array. Symbols are as from Figure 1. End-member compositions are given in Table 3.

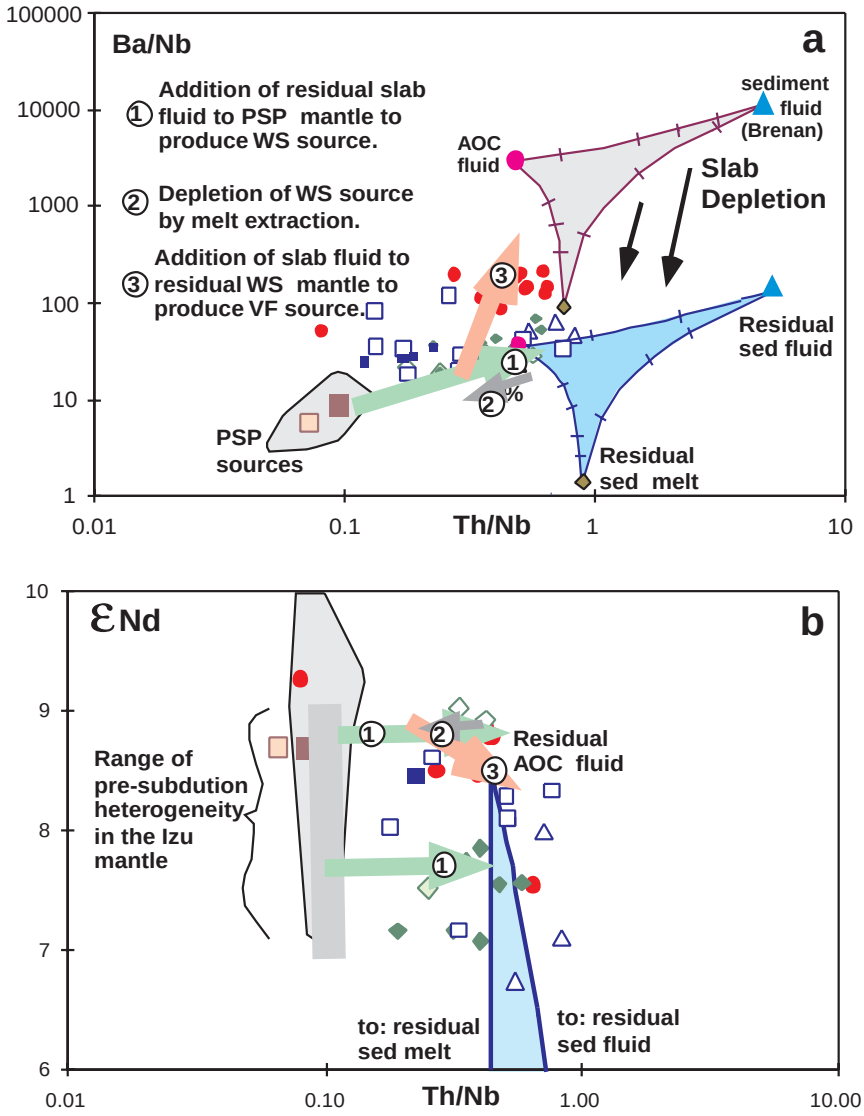

Figure 14. Arrows illustrate three-step model to explain all of the Izu lavas. Model involves Nd isotopic heterogeneity between the WS and VF protoliths and implies that the PSP mantle that enters the rear of the Izu-Bonin mantle wedge is heterogeneous. The most isotopically enriched portions melt beneath the WS, and the isotopically depleted portions melt beneath the VF. Fluids derived from the residual slab (from Figure 13) enter the mantle wedge in the first step. Step two is melting and mantle wedge depletion in all incompatible elements (following *Hochstaedter et al.* [2000]). Step three is addition of slab fluids beneath the VF (from Figure 10). Symbols are as from from 1.

[45] Other sediment indicators, such as Ce/Ce*, are also inconsistent with sediment melt in the WS but not VF. Ce/Ce* values in Izu-Bonin volcanic rocks average ~0.92 (Figure 12), PSP basalts average ~1.0 [*Hickey-Vargas*, 1998], and the average Izu sediment mixture used in this study is ~0.62 (Tables 2 and 3). However, Ce/Ce* does not correlate with other sediment proxies, such as ε_{Nd}, Th/Nb, or Th/Nd, and mixing lines between slab derived components

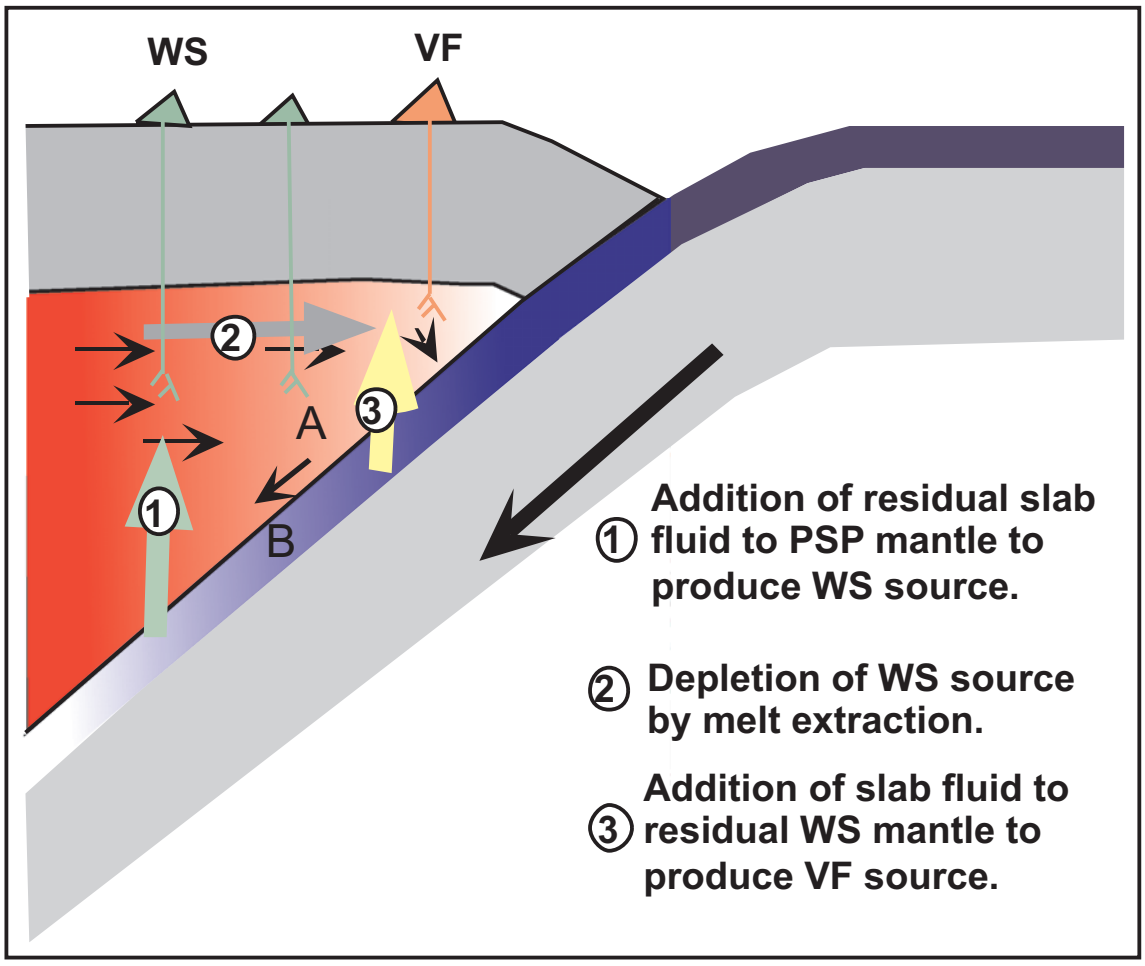

Figure 15. Cartoon shows location within the mantle wedge of the three steps of the model described in Figure 14. Darkness of the red shade (region A) represents fertility of the mantle wedge. Darkness of the blue shade (region B) shows "fertility" of the slab with respect to fluid-mobile elements.

and PSP sources miss the Izu-Bonin rocks. However, the ubiquitous low Ce/Ce*, like the ubiquitously high Th/Nb, suggests that a fluid component can transport light REE and Th.

[46] One element ratio that has been interpreted elsewhere as a tracer of sediment melt, Th/Nd, does correlate negatively with ε_{Nd} in the Izu arc. *Class et al.* [2000] found that Th/Nd ratios are higher in WS-like rocks with higher concentrations of more incompatible elements in the Aleutian arc but, nevertheless, are lower than predicted by binary mixing unless the sediment transfer agent was a melt. The Izu arc shows a similar correlation (Figure 9c). However, the Th/Nd ratios of both inbound sediment and erupted rocks are lower in all Izu rocks than in the Aleutians, and the difference in ε_{Nd} between sediment and volcanics is greater. As a result, Figure 9c requires that the Th/Nd ratio for an Izu sediment melt be ~1.0, whereas the ratio calculated for Izu sediment melt using *Johnson and Plank*'s [1999] partition coefficients is an order of magnitude lower (see vertical arrow in Figure 9c). The same quantitative misfit also applies to the Aleutians

but is less severe. We attribute the difference in Th/Nd between VF and WS to mixing with fluid that is derived primarily from AOC. The nearly horizontal arrow in Figure 9c approximates a quantitative mixing line between the PSP source and an AOC-sediment fluid in which the 88:12 proportion of fluid sources is about the same as indicated by the Pb isotopes. The problem is that Th/Nd, like ε_{Nd}, ratios imply more of this fluid in the WS than VF, whereas Pb isotopes imply less. For that reason, Figure 9c also schematically shows the effect of differences in mantle wedge protoliths.

[47] The combination of high Th/Nb and low Ba/Nb, U/Nb, $^{87}Sr/^{86}Sr$, and ε_{Nd} in the WS suite is one of the major challenges in interpreting the origin of these rocks. The Th in the WS suite must come from a subduction component (Figure 8). If the Th comes from sediment melt, the question is why the ε_{Nd} values are not lower and why the WS suite lacks strong correlations between ε_{Nd}, Th/Nb, and Ce/Ce*. If the Th in the WS suite comes from sediment fluid, the question is why the WS suite does not have higher U/Th, Ba/Th, or $^{206}Pb/^{204}Pb$ values.

[48] We see several solutions to this problem. One solution is that the composition of the subduction component could differ from those considered here. The possibility exists, for example, that the subduction component could be a complex mixture of bulk sediments, sediment melts, sediment fluids, or AOC fluids. Even more likely is that different partition coefficients, residual minerals, or percents of fluid and melt apply. The field of potential slab-derived components is large on Figures 9–12. It is possible that within this field a composition exists that satisfies all of the elemental and isotopic constraints. In particular, there may be conditions, such as those at which phase supercriticality is achieved and the differences between "fluid" and "melt" are lost, where Th is as mobile as Ba, U, or Pb. Although no quantitative model combining homogeneous sources satisfactorily explains the Izu data, the current state of uncertainty, illustrated by the difference in predicted element ratios in sediment fluid end-members in Figures 9–12 precludes confidence that one ever will.

[49] Alternatively, the source of the WS protolith may be heterogeneous with respect to ε_{Nd}. PSP basalts, generated far from subduction influence, display a range in ε_{Nd} similar to that of the Izu-Bonin suite (Figure 6) [*Hickey-Vargas*, 1991, 1998]. Preexisting mantle heterogeneity obviates the need for sediment melt in the subduction mix to lower the ε_{Nd} of the WS source. The WS subduction component could then be a fluid that is more enriched in Th and light REE along with the more conventional fluid-mobile elements and less enriched in slab Sr and Pb than at the VF. In this case the slab sources remain constant but the element partitioning changes.

[50] An additional factor is that by the time the slab reaches the WS region, it may be more depleted in conventional fluid-mobile elements than it was beneath the VF, so that the hydrous fluid emanating beneath the WS is no more enriched in Ba, U, and Pb than it is in Th. In this case the slab (both AOC and sediments) continues to dehydrate rather than melt downdip from the volcanic front, thereby changing in composition, while the element partitioning remains constant [*Ryan et al.*, 1995]. Although these enrichments may not be as great as at shallower levels, they may be sufficiently high to raise the Th/Nb, U/Nb, and Ba/Nb values in the source but not change the U/Th or Ba/Th values. Figure 13 and Table 3 provide a quantitative model of this hypothesis. The model assumes that 2% dehydration has depleted the slab in fluid-mobile elements beneath the VF. An additional 2% fluid is again removed from the slab beneath the WS using the depleted or

residual slab composition as a source. Reasonable end-members are shown on the Ba/Nb-Th/Nb diagram, using a fluid derived from both sediments (~12%) and AOC. Note that with this hypothesis the relative proportions of sediment- and AOC-derived fluids do not change between the VF and WS source regions. This proposal of dehydrating a more fertile slab beneath the volcanic front versus residual slab beneath the back arc (our "residual slab" hypothesis) complements our other proposal of melting more fertile mantle beneath the back arc versus residual mantle beneath the volcanic front [*Hochstaedter et al.*, 2000].

[51] Pb isotopic systematics are also consistent with the residual slab idea. Since the only difference between the VF and WS slab components is "fertility" of the slab in terms of fluid-mobile elements, the isotopic compositions do not change as long as both the AOC and overlying sediment dehydrate to the same extent. If sediment melt rather than sediment fluid plays an important role, then the mixture between sediment melt and AOC fluid beneath the WS must have exactly the same Pb isotopic composition as the mixture between sediment- and AOC-derived fluid beneath the VF, so that the singular trend on the Pb isotope diagram is preserved. The convergence of two different mixtures from the subducting slab upon a single Pb isotopic composition would be an extremely unlikely coincidence.

[52] Not all trace element and isotopic systematics support the "depleted slab fluid" hypothesis. The low $^{87}Sr/^{86}Sr$ and $^{206}Pb/^{204}Pb$ values of the WS suite are not easily explained by any hypothesis involving fluids, which would have high Sr and Pb concentrations and elevated isotope ratios. Only sediment melt can explain simultaneously low $^{87}Sr/^{86}Sr$, $^{206}Pb/^{204}Pb$, and ε_{Nd} if Nd is as incompatible in fluid as implied by the D values used here. However, recent field studies suggest that Hf can be mobile in slab fluids (J. D. Woodhead et al., Hafnium isotope evidence for HFSE mobility during subduction zone processes, submtitted to *Earth and Planetary Science Letters*, 2000). If even Hf moves in fluid, can Nd or Th be far behind?

[53] Involvement of residual versus fertile sediment in the genesis of rocks chemically similar to the WS suite has been proposed before [e.g., *Class et al.*, 2000] but as a precursor to sediment melting rather than serial slab dehydration. Separate dehydrations of AOC have been invoked to explain the presence of both ^{238}U and ^{226}Ra excesses in lavas at the Tongan volcanic front [*Turner et al.*, 2000]. We conclude that the difference in inferred composition of the bulk slab components between the VF and WS suites is better explained by a difference in the composition of the slab source (fertile versus residual) than by a difference in the transfer agent (fluid versus melt).

6. Conclusions and Implications

[54] The most fundamental result of this study is that the slab-derived components which metasomatize the volcanic front (VF) and back arc (Western Seamounts (WS)) portions of the mantle wedge differ. The difference between VF and WS is not simply the presence of less slab component or some sediment melt in the WS. Rather, it is a different slab fluid. The slab component that metasomatizes the VF source can be reasonably attributed to a fluid that is derived from both sediment and AOC sources (~12% sediment derived). The component that metasomatizes the WS, however, is not easily reconcilable with quantitative models using the most obvious subduction-related end-members.

[55] Although the low ε_{Nd}, high Th/Nb and Th/Nd, Ce/Ce* < 1, and the relatively smooth calculated slab component composition on multielement diagrams (Figure 8) could indi-

cate the addition of sediment melt to the mantle wedge beneath the WS, we reject that hypothesis for the following reasons. (1) Few of the important sediment proxies listed above correlate with each other along trends from mantle to sediment values. (2) Mixing lines leading to combinations of slab end-members that include average Izu sediments miss the WS field on most isotopic and trace element diagrams. Mixing lines do trend through the WS field on the Sr-Nd isotopic diagram, however. (3) The WS and VF suites plot along the same trend on the Pb isotopic diagram. It is unlikely that mixtures of AOC fluid plus sediment melts versus sediment fluids will result in the same trend on the Pb isotopic diagram given the expected differences in Pb concentration between the end-members.

[56] If we eliminate mixing with sediment melts, then heterogeneity of the sediment fluid or the mantle protolith or both must be responsible for the WS trend. The fluids must be similar yet distinct from those that metasomatize the VF source. They are similar because of the similar trend on Pb isotopic plots but different because of all the reasons that the WS suite differs from the VF suite.

[57] Of all the potential explanations for why the slab component might differ between the VF and WS, we prefer the residual slab hypothesis (Figures 13–15). As fluids dehydrate from the slab, the composition of the slab changes. In the residual slab, ratios of fluid-mobile to non-fluid-mobile elements are lower, but isotopic characteristics remain unchanged. Thus patterns on a multielement diagram would be smoother than those for the first fluid (i.e., the VF fluid) that dehydrated from the subducting slab (Figure 8). Since the isotopic composition is the same, trends on the Pb isotopic diagrams would be the same as for the first fluid, and WS and VF trends would be similar, as is observed.

[58] The residual slab hypothesis does not explain all of the geochemical features of the WS trend. Most important of these is the low ε_{Nd} of the WS trend. If Nd is immobile in fluids, then trends produced by fluids are nearly horizontal on Sr-Nd isotopic diagrams. Thus any hypothesis that involves fluids rather than average Izu sediment requires ε_{Nd} heterogeneity in the source. Another aspect of the WS that the residual slab hypothesis does not explain is the low $^{87}Sr/^{86}Sr$ values of the WS suite. Sr concentrations and $^{87}Sr/^{86}Sr$ values should be high in any slab-derived fluid. Why the $^{87}Sr/^{86}Sr$ values remain low in the WS suite awaits further investigation.

[59] The residual slab hypothesis implies that the WS suite was derived from portions of the mantle that contained lower ε_{Nd} and Zr/Nb values than those portions that produced the VF suite. More enriched portions of the mantle with lower ε_{Nd} values probably melted first, mostly by decompression, as the mantle entered the rear of the mantle wedge. In contrast, the greater role of fluids and the more refractory source at the VF indicate a greater role of flux melting there.

[60] Our preferred residual slab hypothesis describes Izu-Bonin magmatism in three steps (Figures 14 and 15), beginning with the influx of PSP mantle into the Izu-Bonin mantle wedge. In the first step, fluid from the depleted slab enters the mantle wedge to metasomatize the PSP mantle into the WS source. During this step the fluid from the residual slab metasomatizes both enriched (low ε_{Nd}) and depleted (high ε_{Nd}) portions of the PSP mantle. In the second step, melting occurs which depletes WS mantle, leaving the WS residue. This residue convects toward the volcanic front. In the third step, fluid from a relatively fertile slab enters the mantle wedge, transforming the WS residue into the VF source, which melts to produce the VF suite of magmas (Figures 14 and 15).

[61] In summary, we conclude that both the mantle wedge and slab components differ across the Izu-Bonin arc. The residual slab hypothesis suggested here complements our earlier conclusion [*Hochstaedter et al.*, 2000] that the differences between the WS and VF protoliths were produced by melt extraction in the Izu-Bonin mantle wedge during the most recent subduction phase despite the absence of back arc spreading. We also recognized, however, that presubduction mantle heterogeneity may have been a contributing factor. *Hochstaedter et al.* [2000] emphasized differences in Nb/Zr across the Izu-Bonin arc. This variation occurs mostly between the VF and the rest of the arc. In contrast, the differences in ε_{Nd} that must predate recent subduction occur mostly between the WS and the rest of the arc. Thus presubduction heterogeneity manifests itself today as the enriched ε_{Nd} in some WS volcanic rocks. Much of the non-slab-related heterogeneity, as seen by variation in Nb/Zr, is most evident as the extremely depleted VF compositions. This heterogeneity was probably produced within the Izu-Bonin mantle wedge during the Neogene phase of subduction, as advocated by *Hochstaedter et al.* [2000].

Acknowledgments

[62] We thank Adam Klaus for the bathymetric data in Figure 1b. Senior theses by UCSC undergraduates Yvonne Rodriguez, Kari Fox, and Danika Mullen contributed to our understanding of Izu Arc petrology. We thank the officers, crew, and onboard scientists of the R/V *Moana Wave*. Reviews by Mary Reid, Bill White, Cornelia Class, and an anonymous reviewer improved the presentation and content of the manuscript. This work was supported by NSF grant OCE-9402984.

References

Ayers, J., Trace element modeling of aqueous fluid-peridotite interaction in the mantle wedge of subduction zones, *Contrib. Mineral. Petrol.*, *132*, 381–398, 1998.

Ayers, J. C., S. K. Dittmer, and G. D. Layne, Partitioning of elements between peridotite and H_2O at 2.0–3.0 GPa and 900–1100°C, and application to models of subduction zone processes, *Earth Planet. Sci. Lett.*, *150*, 381–398, 1997.

Ben Othman, D., W. M. White, and J. Patchett, The geochemistry of marine sediments, island arc magma genesis and crust-mantle recycling, *Earth Planet. Sci. Lett.*, *94*, 1–21, 1989.

Brenan, J. M., H. F. Shaw, D. L. Phinney, and F. J. Ryerson, Rutile-aqueous fluid partitioning of Nb, Ta, Hf, Zr, U and Th: Implications for high field strength element depletions in island-arc basalts, *Earth Planet. Sci. Lett.*, *128*, 327–339, 1994.

Brenan, J. M., H. F. Shaw, F. J. Ryerson, and D. L. Phinney, Mineral-aqueous fluid partition of trace elements at 900°C and 2.0 GPa: Constraints on the trace element chemistry of mantle and deep crustal fluids, *Geochim. Cosmochim. Acta*, *59*, 3331–3350, 1995a.

Brenan, J. M., H. F. Shaw, and F. J. Ryerson, Experimental evidence for the origin of lead enrichment in convergent-margin magmas, *Nature*, *378*, 54–56, 1995b.

Class, C., D. M. Miller, S. L. Goldstein, and C. H. Langmuir, 2000.Distinguishing melt and fluid subduction components in Umnak Volcanics, Aleutian arc, *Geochem. Geophys. Geosyst.*, vol. 1, Paper number 1999GC000010 [15,355 words, 11 figures, 5 tables]. June 1, 2000.

Davidson, J. P., Deciphering mantle and crustal signatures in subduction zone magmatism, in *Subduction: Top to Bottom, Geophys. Monogr. Ser.*, vol. 96, edited by G. E. Bebout et al., pp. 251–262, AGU, Washington, D. C., 1996.

Elliott, T., T. Plank, A. Zindler, W. White, and B. Bourdon, Element transport from subducted slab to juvenile crust at the Mariana arc, *J. Geophys. Res.*, *102*, 14,991–15,019, 1997.

Fryer, P., B. Taylor, C. H. Langmuir, and A. G. Hochstaedter, Petrology and geochemistry of lavas from the Sumisu and Torishima back arc rifts, *Earth Planet. Sci. Lett.*, *100*, 161–178, 1990.

Fujimaki, H., and H. Kurasawa, Lateral variation of REE pattern of basaltic magma across the Japan arc, *J. Jpn. Mineral. Petrol. Econ. Geol.*, *75*, 313–322, 1980.

Gill, J. B., *Orogenic Andesites and Plate Tectonics,* 390 pp., Springer-Verlag, New York, 1981.

Gill, J. B., and R. Williams, Th isotope and U-series studies of subduction-related volcanic rocks, *Geochim. Cosmochim. Acta*, *54*, 1427–1442, 1990.

Gill, J. B., C. Seales, P. Thompson, A. G. Hochstaedter, and C. Dunlap, Petrology and geochemistry of Plio-Pleistocene volcanic rocks from the Izu arc and Sumisu Rift, *Proc. Ocean Drill. Program Sci. Results*, *126*, 383–404, 1992.

Gill, J. B., R. N. Hiscott, and P. Vidal, Turbidite geochemistry and evolution of the Izu-Bonin arc and continents, *Lithos*, *33*, 135–168, 1994.

Hart, S. R., A large-scale isotope anomaly in the Southern Hemisphere mantle, *Nature*, *309*, 753–757, 1984.

Hickey-Vargas, R., Isotope characteristics of submarine lavas from the Philippine Sea: Implications for the origin of arc and basin magmas of the Philippine tectonics plate, *Earth Planet. Sci. Lett.*, *107*, 290–304, 1991.

Hickey-Vargas, R., Origin of the Indian Ocean-type isotopic signature in basalts from Philippine Sea plate spreading centers: An assessment of local versus large-scale processes, *J. Geophys. Res.*, *103*, 20,963–20,979, 1998.

Hochstaedter, A. G., J. B. Gill, S. Kusakabe, S. Newman, M. Pringle, B. Taylor, and P. Fryer, Volcanism in the Sumisu Rift, I, Major element, volatile and stable isotope geochemistry, *Earth Planet. Sci. Lett.*, *100*, 179–194, 1990a.

Hochstaedter, A. G., J. B. Gill, and J. D. Morris, Volcanism in the Sumisu Rift, II, Subduction and non-subduction related components, *Earth Plant. Sci. Lett.*, *100*, 195–209, 1990b.

Hochstaedter, A. G., J. B. Gill, B. Taylor, O. Ishizuka, M. Yuasa, and S. Morita, Across-arc geochemical trends in the Izu-Bonin arc: Constraints on source composition and mantle melting, *J. Geophys. Res.*, *105*, 495–512, 2000.

Honza, E., and K. Tamaki, The Bonin Src, in *The Ocean Basins and Margins*, vol. 7, *The Pacific Ocean*, edited by A. E. M. Nairn and S. Uyeda, pp. 459–502,Plenum, New York, 1985.

Ikeda, Y., and M. Yuasa, Volcanism in nascent back-arc basins behind the Shichito Ridge and adjacent areas in the Izu-Ogasawara arc, northwest Pacific: Evidence for mixing between E-type MORB and island arc magmas at the initiation of back-arc rifting, *Contrib. Mineral. Petrol.*, *101*, 377–393, 1989.

Ishizuka, O., K. Uto, M. Yuasa, and A. G. Hochstaedter, Preliminary K-Ar ages from seamount chains in the back-arc region of the Izu-Ogasawara arc, *Island Arc*, *7*, 408–421, 1998.

Johnson, M. C., and T. Plank, 1999.Dehydration and melting experiments constrain the fate of subducted sediments, *Geochem. Geophys. Geosyst.*, vol. 1, Paper number 1999GC000014 [13,479 words, 10 figures, 8 tables]. December 16, 2000.

Kincaid, C., and I. S. Sacks, Thermal and dynamical evolution of the upper mantle in subduction zones, *J. Geophys. Res.*, *102*, 12,295–12,315, 1997.

Klaus, A., B. Taylor, G. F. Moore, M. MacKay, Y. Okamura, and F. Murakami, Backarc rifting in the Izu-Bonin Island arc: Structural evolution of Hachijo and Aoga Shima Rifts, *Island Arc*, *1*, 16–31, 1992.

Leeman, W. P., Boron and other fluid-mobile elements in volcanic arc lavas: Implications for subduction processes, in *Subduction: Top to Bottom, Geophys. Monogr. Ser.*, vol. 96, edited by G. E. Bebout et al., pp. 269–276, AGU, Washington, D. C., 1996.

Leeman, W. P., M. J. Carr, and J. D. Morris, Boron geochemistry of the Central American volcanic arc: Constraints on the genesis of subduction-related magmas, *Geochim. Cosmochim. Acta*, *58*, 149–168, 1994.

Lin, P.-N., Trace element and isotopic characteristics of western Pacific pelagic sediments: Implications for the petrogenesis of Mariana arc magmas, *Geochim. Cosmochim. Acta*, *56*, 1641–1654, 1992.

Morita, S., Topography, geologic structures and geochemical variations of the northern Izu-Bonin arc, M.S. thesis, 58 pp. Ocean Res. Inst., Univ. of Tokyo, Tokyo, 1994.

Morris, J., and F. Tera, $^{10}Be/^{9}Be$ in mineral separates and whole rocks from volcanic arcs: Implications for sediment subduction, *Geochim. Cosmochim. Acta*, *53*, 3197–3206, 1989.

Niu, Y., and R. Batiza, Trace element evidence from seamounts for recycled oceanic crust in the eastern Pacific mantle, *Earth Planet. Sci. Lett.*, *148*, 471–483, 1997.

Pearce, J. A., and I. J. Parkinson, Trace element models for mantle melting: Application to volcanic arc petrogenesis, in *Magmatic Processes and Plate Tectonics*, edited by H. M. Prichard et al., *Geol. Soc. Spec. Publ., 76*, 373–403, 1993.

Plank, T., and C. H. Langmuir, Tracing trace elements from sediment input to volcanic output at subduction zones, *Nature*, *362*, 739–742, 1993.

Plank, T., and J. Ludden, Geochemistry of sediments in the Argo abyssal plain at Site 765: A continental margin reference section for sediment recycling in subduction zones, *Proc. Ocean Drill. Program Sci. Results*, *123*, 167–189, 1992.

Plank, T., J. Ludden, C. Escutia, and Shipboard Science Party, *Preliminary Summary of Drilling Results of the Ocean Drilling Program, Leg 185*, 987 pp., Ocean Drill. Program, College Station, Tex., 1999.

Ryan, J. G., J. D. Morris, F. Tera, W. P. Leeman, and A. Tsvetkov, Cross-arc geochemical variations in the Kurile arc as a function of slab depth, *Science*, *270*, 625–627, 1995.

Stalder, R., S. F. Foley, G. P. Brey, and I. Horn, Mineral-aqueous fluid partitioning of trace elements at 900–1200°C and 3.0–5.7 GPa: New experimental data for garnet, clinopyroxene, and rutile, and implications for mantle metasomatism, *Geochim. Cosmochim. Acta*, *62*, 1781–1801, 1998.

Staudigel, H., T. Plank, B. White, and H.-U. Schmincke, Geochemical fluxes during seafloor alteration of the basaltic upper oceanic crust: DSDP Sites 417 and 418, in *Subduction: Top to Bottom, Geophys. Monogr. Ser.*, vol. 96, edited by G. E. Bebout et al., pp. 19–38, AGU, Washington, D. C., 1996.

Stern, R. J., J. Morris, S. B. Bloomer, and J. W. Hawkins, The source of the subduction component in convergent margin magmas: Trace element and radiogenic isotope evidence from Eocene boninites, Mariana forearc, *Geochim. Cosmochim. Acta*, *55*, 1467–1481, 1991.

Straub, S. M., Miocene to Quaternary evolution of the Izu Bonin island arc, *Eos Trans. AGU*, *77*(46), Fall Meet Suppl., F842, 1996.

Sun, S. S., and W. F. McDonough, Chemical and isotopic systematics of oceanic basalts: Implications for mantle composition and processes, in *Magmatism in the Ocean Basins*, edited by A. D. Saunders and M. J. Norry, *Geol. Soc. Spec. Publ.*, *42*, 313–345, 1989.

Takada, A., F. Murakami, and M. Yuasa, Geological maps of volcanoes, 7, Aogashima volcano and submarine volcanoes, south of Izu islands, Geol. Surv. of Jpn., Tsukuba, 1994.

Tatsumi, Y., M. Murasake, and S. Nohda, Across-arc variation of lava chemistry in the Izu-Bonin arc: Identification of subduction components, *J. Volcanol. Geotherm. Res.*, *49*, 179–190, 1992.

Taylor, B., Rifting and the volcanic-tectonic evolution of the Izu-Bonin-Mariana arc, *Proc. Ocean Drill. Program Sci. Results*, *126*, 627–652, 1992.

Taylor, B., G. Brown, P. Fryer, J. Gill, A. Hochstaedter, H. Hotta, C. Langmuir, M. Leinen, A. Nishimua, and T. Urabe, Alvin-SeaBeam studies of the Sumisu Rift, Izu-Bonin arc, *Earth Planet. Sci. Lett.*, *100*, 127–147, 1990.

Taylor, R. N., and R. W. Nesbitt, Isotopic characteristics of subduction fluids in an intra-oceanic setting, Izu-Bonin arc, Japan, *Earth Planet. Science Lett.*, *164*, 79–98, 1998.

Tera, F., L. Brown, J. Morris, and I.S. Sacks, Sediment incorporation in island-arc magmas: Inferences from ^{10}Be, *Geochim. Cosmochim. Acta*, *50*, 535–550, 1986.

Todt, W., R. Cliff, A. Hanser, and A. Hofmann, ^{202}Pb + ^{205}Pb double spike for lead isotopic analysis, *Terra Cognita*, *4*, 209, 1984.

Turner, S., C. Hawkesworth, N. Rogers, J. Bartlett, T. Worthington, J. Hergt, J. Pearce, and I. Smith, ^{238}U-^{230}Th disequilibria, magma petrogenesis, and flux rates beneath the depleted Tonga-Kermadec island arc, *Geochim. Cosmochim. Acta*, *61*, 4855–4884, 1997.

Turner, S., B. Bourdon, C. Hawkesworth, and P. Evans, ^{226}Ra-^{230}Th evidence for multiple dehydration events, rapid melt ascent and the time scales of differentiation beneath the Tonga-Kermadec island arc, *Earth Planet. Sci. Lett.*, *179*, 581–593, 2000.

Yuasa, M., and M. Nohara, Petrographic and geochemical along-arc variations of volcanic rocks on the volcanic front of the Izu-Ogasawara (Bonin) Arc, *Bull. Geol. Surv. Jpn.*, *43*, 421–456, 1992.

Woodhead, J. D., S. M. Eggins, and R. W. Johnson, Magma genesis in the New Britain Island arc: Further insights into melting and mass transfer processes, *J. Petrol.*, *39*, 1641–1668, 1998.